JOURNAL OF PETROLOGY

Journal of Petrology, 2019, Vol. 60, No. 1, 117–150
doi: 10.1093/petrology/egy108
Advance Access Publication Date: 5 December 2018
Original Article

OXFORD

Evolution of Alkalic Magma Systems: Insight from Coeval Evolution of Sodic and Potassic Fractionation Lineages at The Pleiades Volcanic Complex, Antarctica

Jihyuk Kim[1]*, Jung-Woo Park[1], Mi Jung Lee[2], Jong Ik Lee[2] and Philip R. Kyle[3]

[1]School of Earth and Environmental Sciences, Seoul National University, 1 Gwanak-ro, Seoul 08826, Republic of Korea; [2]Division of Polar Earth System Sciences, Korea Polar Research Institute (KOPRI), 26 Songdomirae-ro, Incheon 406-840, Republic of Korea; [3]Department of Earth and Environmental Science, New Mexico Institute of Mining and Technology, 801 Leroy Place, Socorro, NM 87801, USA

*Corresponding author. School of Earth and Environmental Sciences, Seoul National University, Seoul 08826, Republic of Korea. Telephone: +82 2 880 8125. E-mail: jihyuk008@snu.ac.kr

Received May 31, 2018; Accepted November 19, 2018

ABSTRACT

The magmatic evolution of The Pleiades, a Quaternary alkalic volcanic complex in Northern Victoria Land (NVL), Antarctica, is investigated using major and trace element, and Sr, Nd and Pb isotopic data. The volcanic rocks can be subdivided into two distinct magmatic lineages based on petrography and whole-rock compositions: (1) a sodic silica-undersaturated lineage with abundant kaersutite phenocrysts and (2) a potassic and mildly-alkalic, silica-saturated to slightly undersaturated lineage containing olivine phenocrysts but no kaersutite. The pressure–temperature paths estimated by clinopyroxene–liquid thermobarometry are similar in each lineage. Mass-balance calculations using whole-rock and mineral compositions show that kaersutite fractionation without olivine has played a major role in magmatic differentiation of the sodic lineage, whereas the compositional variations of the potassic lineage can be ascribed to fractionation of an assemblage of plagioclase, clinopyroxene, olivine, titanomagnetite and apatite, combined with about 10% lower crustal assimilation. The higher $^{87}Sr/^{86}Sr$ ($> 0{\cdot}7035$), lower $^{143}Nd/^{144}Nd$ ($< 0{\cdot}51285$), and $^{206}Pb/^{204}Pb$ ($< 19{\cdot}3$) ratios of the evolved potassic lavas compared to the mafic lavas support crustal assimilation. The mafic lavas from both lineages are characterized by elevated $^{206}Pb/^{204}Pb$ ($>19{\cdot}5$) ratios and narrow ranges of $^{87}Sr/^{86}Sr$ ($0{\cdot}70313$–$0{\cdot}70327$) and $^{143}Nd/^{144}Nd$ ($0{\cdot}51289$–$0{\cdot}51290$) ratios, which is consistent with a high μ-like (HIMU, where $\mu=(^{238}U/^{204}Pb)_{t=0}$) component typical of Cenozoic volcanic rocks in Antarctica and Zealandia. This HIMU-like isotopic signature of The Pleiades volcanic rocks, together with elevated Nb concentrations and negative K anomalies in primitive mantle-normalized diagrams, suggests an amphibole-bearing metasomatized lithospheric mantle source. We suggest that the primary magmas of the two lineages were formed by partial melting of metasomatic hydrous veins in the lithospheric mantle with varying degrees of reaction with the surrounding, anhydrous peridotite. The drier potassic magma experienced greater peridotite assimilation relative to the more hydrous sodic magmas. This hypothesis is supported by lower contents of Al_2O_3, TiO_2, K_2O, Rb, and Nb in the mafic potassic lavas compared to the sodic ones. This initial difference was intensified by crustal assimilation in the potassic magma suite, resulting in a silica-saturated alkalic trend which is distinct from the trend of the sodic silica-undersaturated alkalic magmas.

Key words: alkalic magmatism; crustal contamination; fractional crystallization; partial melting; The Pleiades Volcanic Complex; McMurdo Volcanic Group

INTRODUCTION

Alkalic volcanic rocks occur in a variety of intraplate tectonic settings and they show a number of evolutionary differentiation trends. The settings include: oceanic islands (e.g. St. Helena, Baker, 1969; Iceland, Jakobsson *et al.*, 1973; Tristan da Cunha, Le Roex *et al.*, 1990; Freundt & Schmincke, 1995); continental rifts (e.g. West Antarctic Rift System, Kyle, 1990a; East African Rift System, Jung & Hoernes, 2000; Rogers, 2006; Lucassen *et al.*, 2013; Rhine Graben rift system, Jung *et al.*, 2012); extensional back-arc basins (e.g. Deception Island, Weaver *et al.*, 1979; Ukinrek Maars, Kienle *et al.*, 1980; Ulleung Island, Brenna *et al.*, 2014), and other intraplate environments (Coombs & Wilkinson, 1969; Ayuso *et al.*, 1998; Kuritani *et al.*, 2009; Correale *et al.*, 2014). The magmatic differentiation of alkalic volcanic suites can be subdivided into fractionation lineages (Coombs & Wilkinson, 1969). The silica-saturated to mildly-undersaturated lineage ranges from alkali basalt and hawaiite to mugearite, benmoreite and trachyte, and occasionally to alkalic rhyolite. The alkali-enriched, strongly silica-undersaturated lineage evolves from basanite, tephrite and rarely hawaiite through phonotephrite, tephriphonolite to phonolite. Volcanic suites can further be subdivided into sodic ($K_2O/Na_2O < 2$) and potassic trends ($K_2O/Na_2O > 2$). Although compositional variations in many volcanoes can be explained by a single trend, there are volcanoes in which two spatially and temporally related evolutionary trends coexist (Cantal volcano, Wilson *et al.*, 1995; Mount Sidley, Panter *et al.*, 1997; Pribilof Islands, Chang *et al.*, 2009; Mount Morning, Martin *et al.*, 2010; Siebengebirge, Kolb *et al.*, 2012).

The causes of such diversity in alkalic magmatism, especially in a single volcanic system, are a matter of debate. Green (1973*a*) attributed it partly to the nature of the parental basaltic magmas which form by varying degrees of partial melting of mantle peridotite. However, decades of studies have shown that the different physiochemical conditions, such as pressure and volatile contents, and consequently different fractionating mineral assemblages (e.g. Coombs & Wilkinson, 1969; Wilson *et al.*, 1995; Nekvasil *et al.*, 2004; Whitaker *et al.*, 2006) or crustal assimilation (e.g. Foland *et al.*, 1993; Schneider *et al.*, 2016), can also affect the degree of silica-undersaturation during the evolution of alkalic magmas. Moreover, various melting processes of distinct mantle lithologies have been proposed to explain alkalic magma genesis: asthenospheric garnet peridotite (Green, 1973*b*; Baasner *et al.*, 2016); pyroxenite (Sobolev *et al.*, 2005); amphibole- or phlogopite-bearing lithospheric mantle (Class & Goldstein, 1997; Pilet *et al.*, 2008), with or without addition of hydrous or carbonate fluids. Experimental studies have shown the importance of carbonate-rich volatiles in the mantle source during partial melting processes (Hirose, 1997; Dasgupta *et al.*, 2007; Gerbode & Dasgupta, 2010). Those sources are closely linked to regional tectonic history and structures as well as the initial physiochemical conditions for partial melting.

The Pleiades are a young volcanic complex in NVL, Antarctica (Fig. 1). They are part of the extensive Cenozoic McMurdo Volcanic Group (Kyle, 1990*b*; Wilson *et al.*, 2002) in the western Ross Sea. Magmas with diverse composition ranging from alkali basalt and basanite to trachyte and phonolite have erupted through the thick crust of the Transantarctic Mountains (TAM) for $\sim$ 1 Ma at The Pleiades (Esser & Kyle, 2002). Two magmatic differentiation lineages (sodic vs potassic) have been identified at The Pleiades based on their marked chemical differences in the intermediate lava suites (Kyle, 1982). The sodic lineage lavas are basanite, tephrite, phonotephrite and tephriphonolite, whereas the potassic lineage consists of hawaiite, mugearite, trachyte, and phonolite. Kyle & Rankin (1976) also noted that the phenocryst assemblages within the two lineages are different. The sodic lineage resembles the kaersutite (Ti-rich calcic amphibole)-bearing basanite–phonolite lineage seen in the Dry Valley Drilling Project (DVDP) core drilled at Hut Point Peninsula on Ross Island (Kyle, 1981). Kaersutite is however rare in the potassic lineage. At The Pleiades, the eruptive ages, localities and compositional variations in the mafic suites of the two lineages overlap (Kyle, 1982; Esser & Kyle, 2002). The Pleiades lavas, therefore, provide an opportunity to examine processes that produced the two contrasting fractionation trends. In this study, we report a new set of mineralogical data, major and trace element data, and isotopic data for The Pleiades volcanic rocks of both lineages, and selected basement rocks. We examine partial melting and differentiation processes and provide petrogenetic models for the two contrasting lineages in The Pleiades.

TECTONIC FRAMEWORK

NVL consists of three major terranes accreted during the Cambro–Ordovician Ross Orogeny (Federico *et al.*, 2006): the Wilson, Bowers and Robertson Bay terranes (Fig. 1b). The terranes are bounded by the northwest–southeast striking Lanterman and Leap Year Faults and mainly consists of pelitic metamorphic rocks and sedimentary rocks (Cooper *et al.*, 1983; Palmeri, 1997; Henjes-Kunst & Schüssler, 2003). The Cambrian to early Ordovician Granite Harbour Intrusive Complex (GHIC) and the Devonian to early Carboniferous Admiralty Intrusives (AI) are widely distributed in NVL (Borg *et al.*, 1987). The syn- and post-tectonic intrusions of the

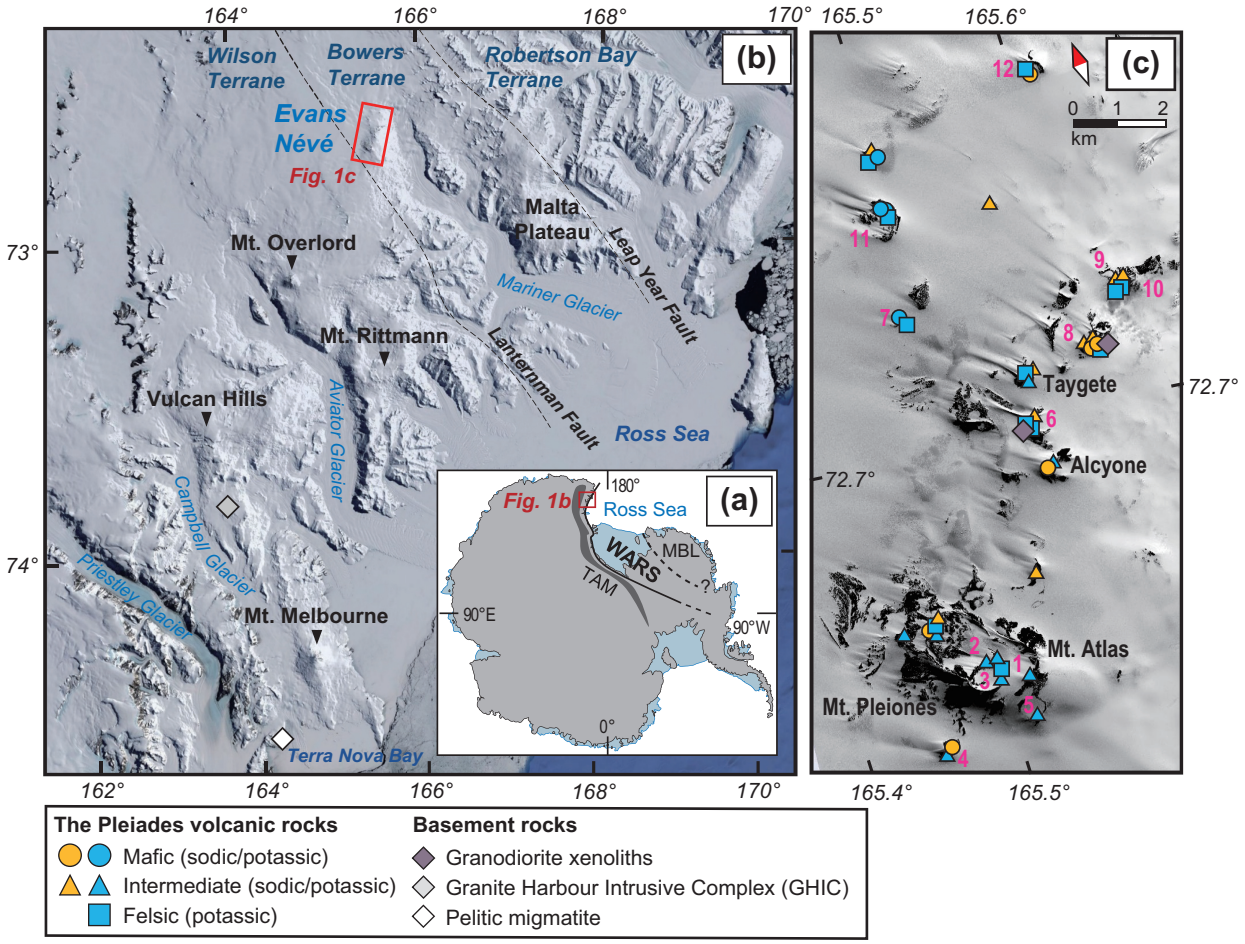

Fig. 1. (a) Distribution and location of the West Antarctic Rift System (WARS), Marie Byrd Land (MBL), and Transantarctic Mountains (TAM) in Antarctica. Grey and blue areas denote continent and ice shelf, respectively. (b) Satellite view of part of Northern Victoria Land (NVL) from Google Earth showing the location of The Pleiades (red box) on the crest of the Transantarctic Mountains. The sample locations of migmatite and Granite Harbour Intrusive Complex (GHIC), are shown. The Lanterman and Leap Year Faults mark the boundaries between the Wilson, Bowers, and Robertson Bay terranes. (c) Satellite view of The Pleiades volcanic complex (World-View image) showing the volcanic rock and xenolith sample locations. The numbered (1–12) and named (Alcyone and Taygete) cones and the two Peaks (Atlas and Pleiones) are marked (Kyle, 1982).

GHIC, which were formed during the Ross Orogeny, occur throughout the TAM, including the Wilson and Bowers terranes (Armienti *et al.*, 1990). The AI occur only in the Robertson Bay and Bowers terranes as Devonian 'stitching granitoids' (Weaver *et al.*, 1984).

The West Antarctic Rift System (WARS; Behrendt, 1999; Fig. 1a) developed major basins in the Ross Sea from late Cretaceous to early Tertiary times (Decesari *et al.*, 2007; Elliot, 2013). A sharp topographical contrast exists between the thin (~20 km) Ross Sea and the thick (~40 km) TAM crust (Chaput *et al.*, 2014; Hansen *et al.*, 2016) which has been attributed to the uplift of the TAM as a rift shoulder of the WARS (Behrendt, 1999). Recent geophysical studies around Victoria Land suggest that the TAM is supported by thermally buoyant, low-velocity mantle zones in which rift-related partial melting has occurred (Graw *et al.* 2016; Hansen *et al.* 2016; Brenn *et al.*, 2017).

Multiple suites of Cenozoic alkalic plutons, dykes and volcanic rocks have been emplaced in and adjacent to the WARS since 48 Ma in NVL and 34 Ma in Marie Byrd Land (MBL) (Rocchi *et al.*, 2002, 2006). Studies of terrestrial volcanic rocks, marine sediments and ice-core tephra layers have confirmed that the volcanism in the Melbourne volcanic province was active from Miocene to Holocene times (Kyle, 1990*a*; Armienti & Baroni, 1999; Narcisi *et al.*, 2012; Del Carlo *et al.*, 2015). A mantle plume beneath the WARS has been suggested as the source of the young alkalic magmatism, based on its ocean island basalt (OIB)-like geochemical characteristics, the volume of volcanic rocks, the dome-shaped elevation of the MBL, seismic data, and high heat flow (Hole & LeMasurier, 1994; Behrendt, 1999; Storey *et al.*, 1999; Sieminski *et al.*, 2003; Winberry & Anandakrishnan, 2004; Schroeder *et al.*, 2014). However, non-plume models have also been

introduced to explain NVL volcanism. Rocchi *et al.* (2005) suggested that transtensional, oblique rifting has promoted Cenozoic NVL magmatism. This oblique rifting was controlled by reactivation of preexisting north to northwest-striking fault systems in conjunction with the movement of fracture zones in the Southern Ocean (Rocchi *et al.*, 2002, 2005; Storti *et al.*, 2006, 2007, 2008; Vignaroli *et al.*, 2015). The non-plume model attributes the geochemical characteristics of the alkalic volcanic rocks around NVL to partial melting of metasomatized lithospheric mantle which has been heated by lateral asthenospheric mantle flow (Nardini *et al.*, 2009; Panter *et al.*, 2018). Hansen *et al.* (2014) reported a slow velocity anomaly beneath the TAM without a deep root ($<$ 300 km), which supports a passive rift model for NVL. Recently, Shen *et al.* (2018) proposed that the slow velocity zone beneath the southern TAM was derived by lithospheric foundering and lateral flow of asthenosphere.

VOLCANIC GEOLOGY

Cenozoic alkalic volcanic rocks in the western Ross Sea area are termed the McMurdo Volcanic Group (Kyle, 1990*b*). The McMurdo Volcanic Group is divided into three provinces: Hallett, Melbourne, and Erebus. The Pleiades are part of the Melbourne volcanic province (Kyle, 1990*a*) which stretches from Mt. Melbourne on the coast, inland to The Pleiades (Fig. 1b) and beyond.

The Pleiades are bounded to the northwest by the Evans Névé (Fig. 1b) and surrounded by a variety of basement rocks, including the sedimentary rocks of the Bowers Terrane, Paleozoic granitoid rocks of both the Granite Harbour Intrusive Complex (GHIC) and Admiralty Intrusives, Mesozoic Ferrar Group tholeiitic volcanic and intrusive rocks, and metamorphic rocks of the Wilson Terrane. The Pleiades itself consists of a stratovolcano and numerous volcanic cones and domes (Kyle, 1986). Those cones are aligned in a roughly northeast–southwest direction, perpendicular to the major strike-slip fault patterns of NVL. There are four named features and twelve unnamed cones which are numbered C1 to C12 (Kyle, 1982; Fig. 1c). The southern peaks of Mt. Pleiones and Mt. Atlas are parts of a single stratovolcano, which is the largest feature of The Pleiades. The Pleiones/Atlas stratovolcano rises $\sim$ 500 m above Evans Névé at the southern end of The Pleiades complex, surrounded by several smaller cinder cones, lava flows and moraines.

The Pleiades has long been thought to be one of the youngest volcanic centers in the McMurdo Volcanic Group based on the undissected nature of the volcanic bodies (Nathan & Schulte, 1968; Riddolls & Hancox, 1968) and geochronology data (Armstrong, 1978; Esser & Kyle, 2002). For example, Taygete Cone is suggested to be a very young endogenous dome based on well-preserved slickensides, rock textures and morphology (Kyle, 1982), and has an $^{40}Ar/^{39}Ar$ age of 6 ± 6 (2σ) ka (Esser & Kyle, 2002). Narcisi *et al.* (2001) suspected the composition of a 1254 ± 2 CE trachytic tephra layer found in the Talos Dome ice core could have been erupted from Mt. Rittmann or The Pleiades. The Pleiades have also been suspected to be one possible source of other young tephra layers found around Talos Dome and in marine sediments (Del Carlo *et al.*, 2015; Narcisi *et al.*, 2016). Indeed, the $^{40}Ar/^{39}Ar$ age determinations of volcanic rocks from The Pleiades are all less than 1 Ma (Esser & Kyle, 2002).

Kyle & Rankin (1976) proposed two differentiation trends at The Pleiades and subdivided them into potassic ($Na_2O/K_2O < 2$) and sodic ($Na_2O/K_2O > 2$) lineages. The potassic lineage is composed of mildly alkalic hawaiite, mugearite, benmoreite and trachyte suite rocks and constitutes the majority of the eruptive volume. The volumetrically minor sodic lineage comprises strongly silica-undersaturated basanite, phonotephrite, and terphriphonolite lavas.

SAMPLE COLLECTION AND ANALYTICAL METHODS

Samples of The Pleiades volcanic complex were collected during two field campaigns, one in December 2014 and one in January 2016. We sampled various lithologies from exposed cones and moraines (Fig. 1c) and these were taken to be representative of The Pleiades volcanic complex. Mineralogy and petrologic features were examined in thin sections and samples were selected for microprobe analysis. Relative abundances of phenocrysts were measured in representative thin sections by measuring the area of each phenocryst in digitized thin section images. Any samples showing alteration or magma mingling textures were excluded from this study. Selected samples were crushed into chips and ground in a tungsten carbide mill for analysis.

We analysed 67 volcanic rocks, two granodiorite AI xenoliths from The Pleiades (see Supplementary Data S1 for age determination; supplementary data are available for downloading at http://www.petrology.oxfordjournals.org) and two basement rocks (GHIC and migmatite) from near Terra Nova Bay. Major elements were determined by X-ray fluorescence (XRF) at the Korean Polar Research Institute (KOPRI), on a PANalytical Axios Max wavelength dispersive XRF spectrometer equipped with a 4 kW Rh anode Super Sharp X-ray Tube (PW2592). Dried sample powders were mixed with lithium tetraborate ($Li_2B_4O_7$) and lithium bromide (LiBr) and fused into glass discs (Fitton & Godard, 2004; Mori, 2005). Loss on ignition (LOI) was determined from the weight change when an aliquot of the sample was heated to 1000°C. Trace element contents were measured using an inductively coupled plasma mass spectrometer (Perkin-Elmer SCIEX Elan 6100 and iCAP Q) at KOPRI. Powdered samples (20 mg) were dissolved in an HF-HNO_3 mixture for 2 days and diluted to $\sim$2% HNO_3. The analytical accuracy and precision were monitored by multiple measurements of reference material BCR-2.

The standard results for most of the elements are in agreement (<12%), except for Y and Pb (<17%), with the recommended values provided by Jochum *et al.* (2005) (Supplementary Data).

The Sr, Nd and Pb isotopic compositions were measured using the laboratory and analytical procedures reported in Lee *et al.* (2015). Fresh rock chips, 1–2 mm in size, were leached in 2 N HCl at 70°C for 10 minutes and repeatedly rinsed with Milli-Q® water to remove possible remaining contaminants. The leached material was powdered in an agate mortar. The powdered samples were dissolved in concentrated HF and $HClO_4$ at 120°C for about 3 days. The sample size was 50 mg for most samples, but 30 mg for some highly-evolved samples, i.e. phonolite, trachyte and granitic rocks, because of their high concentration of Pb (>15 μg/g or part per million, ppm) than other mafic to intermediate rocks (<10 ppm). An anion exchange column (0·5 mL column volume, Ag1 x8, 100–200 mesh resin) with an HBr medium was used to separate Pb which was collected with 6 N HCl. Strontium was then separated from rare earth element (REE) solutions through columns with Biorad AG50W-X8 (4 mL column volume, 100–200 mesh) resin. The columns with Biorad AG50W-X8 (0·7 column volume, 200–400 mesh) were used with 0·22 M alpha hydroxyisobuteric acid (α-HIBA) to collect Nd from the REE solution (Shibata & Yoshikawa, 2004).

Analyses for Sr, Nd, and Pb isotopes were made at KOPRI on a thermal ionization mass spectrometer (TIMS, Thermo Finnigan, TRITON) equipped with 7 Faraday cups. Fractionations of Sr and Nd isotopes were corrected for by normalizing to $^{86}Sr/^{88}Sr = 0{\cdot}1194$ and $^{146}Nd/^{144}Nd = 0{\cdot}7219$. Replicate measurements of NBS 987 and JNdi-1 standards gave $^{87}Sr/^{86}Sr = 0{\cdot}7102711 \pm 6$ (N = 15, 2σ) and $^{143}Nd/^{144}Nd = 0{\cdot}512105 \pm 2$ (N = 15, 2σ). A lead double-spike technique with Southampton-Brest-Lead 207–204 (SBL74) solution was used to determine Pb isotopic ratios. Replicate analyses of the NBS 981 standard gave mean values of $^{206}Pb/^{204}Pb = 16{\cdot}941 \pm 0{\cdot}002$, $^{207}Pb/^{204}Pb = 15{\cdot}497 \pm 0{\cdot}002$, and $^{208}Pb/^{204}Pb = 36{\cdot}724 \pm 0{\cdot}006$ (N = 17; 2σ). The blanks for Sr, Nd, and Pb were all less than 100 pg, negligible compared to the analysed samples.

The mineralogical compositions of representative samples of each lineage were analysed using a JEOL JXA-8530F field-emission electron probe microanalyser (FE-EPMA) equipped with five wavelength-dispersive spectrometers at KOPRI. Quantitative analyses were performed on carbon-coated thin sections with a focused beam of 3 μm diameter, an accelerating voltage of 15 kV, and a beam current of 15 nA. Peak position and background counting times were 20 and 10 seconds, respectively. Sodium was analysed first to mitigate any loss due to volatilization. Natural minerals and synthetic oxides were used for calibration standards. A suite of Smithsonian microbeam standards was analysed together with unknown samples daily to monitor data quality. All microprobe data were processed using the PRZ-A matrix correction method.

RESULTS

Petrography and field relationships

Most lavas from The Pleiades have seriate or porphyritic textures, with phenocrysts set in a fine-grained, melanocratic groundmass. Vesicularity is variable. Felsic, trachytic lavas can be distinguished from mafic and intermediate lavas in the field by their typical leucocratic colors and almost aphyric nature. The cones and domes of The Pleiades are generally well preserved, but multiple generations of overlapping lava flows obscure the stratigraphic order. The locations of the samples have no recognizable spatial relationship between mafic and felsic rocks or sodic and potassic lineages. Centimetre to decimetre sized xenoliths of cognate essexite and syenite are common.

Sodic lineage

The mafic lavas of the sodic lineage are seriate-textured, with basanite and hawaiite compositions. Olivine, clinopyroxene, kaersutite, plagioclase and Fe–Ti oxide phenocrysts are surrounded by a melanocratic groundmass composed of clinopyroxene, oxides, and plagioclase (Fig. 2a). Euhedral to subhedral clinopyroxene is the most abundant phenocryst (e.g. ~60% of the phenocrysts in the sample K16012708-4). Clinopyroxene often shows sector or discontinuous zonation and contains oxide, sulfide or melt inclusions, particularly in the center of the crystal. In plane-polarized light, some phenocrysts exhibit a pink clinopyroxene rim overgrown on either an olivine core or a green clinopyroxene core. Olivine phenocrysts are mostly euhedral to subhedral, with occasional occurrence as strongly-sieved microphenocrysts. Kaersutite phenocrysts show angular and prismatic shapes and are always mantled by 20–150 μm thick oxide rims. Some kaersutite phenocrysts contain clinopyroxene and oxide inclusions, suggesting that their onset of crystallization is preceded by the latter two phases. Two Si-poor basanite samples (K16012411-1 and K16012412-2) with abundant clinopyroxene (1–5 mm in size) and Fe–Ti oxide phenocrysts are also included in the sodic lineage, although they lack kaersutite. They are distinct from the mafic rocks of the potassic lineage by the absence of olivine phenocrysts. Plagioclase is a minor phenocryst phase and is mostly present in the groundmass or as microphenocrysts (<1 mm).

Lavas of intermediate composition have clinopyroxene, kaersutite and plagioclase phenocrysts set in a leucocratic groundmass (Fig. 2c and e). The abundance of kaersutite phenocrysts increases at the expense of clinopyroxene phenocrysts as the magma evolves from phonotephrite to tephriphonolite. Kaersutite overgrowths on clinopyroxene are commonly observed.

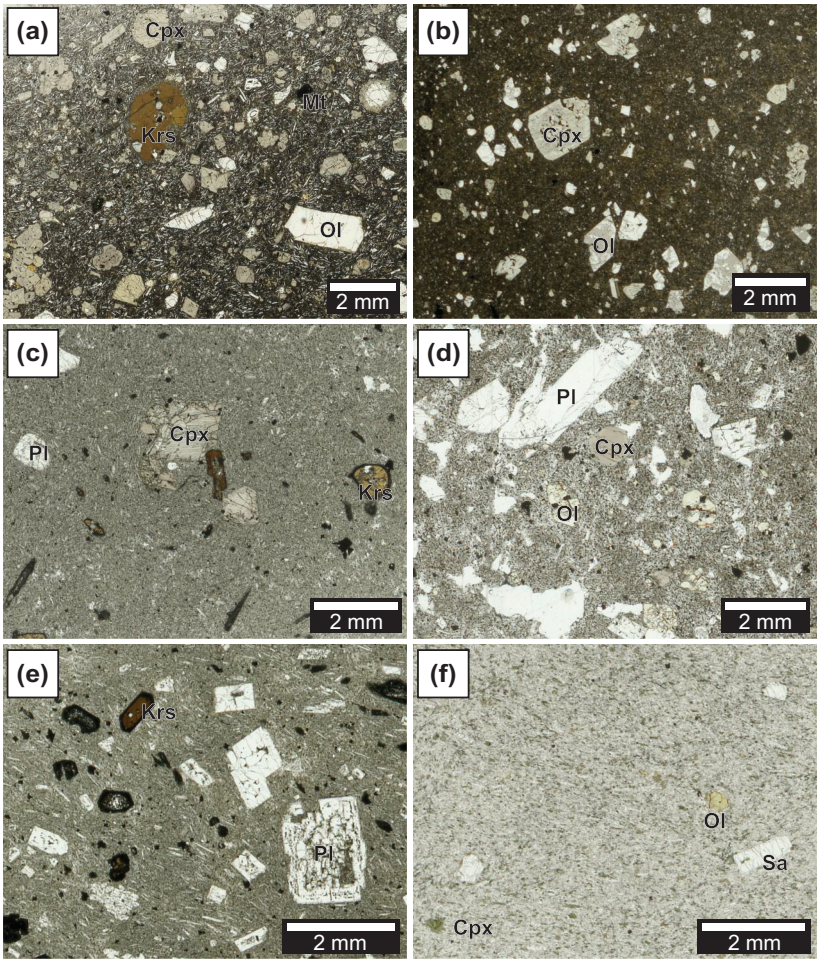

Fig. 2. Representative thin section photographs of the sodic and potassic differentiation series in plane polarized light. (a) Sodic basanite (K16012708-4) containing kaersutite and clinopyroxene with minor olivine, plagioclase, and Fe–Ti oxides. (b) Olivine- and clinopyroxene-phyric potassic hawaiite (K16012424). (c) Sodic phonotephrite (K16012713-2) containing kaersutite and clinopyroxene with less abundant plagioclase and Fe–Ti oxides. (d) Potassic mugearite (K16012708-2) with abundant plagioclase and clinopyroxene, olivine, and oxide (micro)phenocrysts. (e) Sodic tephriphonolite (K16012713-1) with plagioclase, kaersutite, and kaersutite pseudomorphs, and (f) Trachyte (K16012407-1) containing fayalite (Ol), aegirine–augite (cpx), and sanidine (Sa) microphenocrysts. Note the more abundant plagioclase phenocrysts in mugearite (d) compared to the phonotephrite (c). Ol, Olivine; Cpx, clinopyroxene; Mt, (titano)magnetite; Krs, kaersutite; Pl, plagioclase; Sa, sanidine.

Most kaersutite phenocrysts are partially or entirely replaced by oxide rims. The modal abundance of plagioclase phenocrysts increases as the whole-rock composition evolves until they become the dominant phenocryst phase in the most evolved samples. For example, their abundance is <1% among phenocrysts in basanite sample K16012708-4 whereas it is ~75% in the tephriphonolite sample K16012713-1. Nepheline is rare and only occurs as microphenocrysts (0·2–0·3 mm in size) rimmed by plagioclase laths in the most evolved whole-rock compositions.

Potassic lineage

The alkali basalt and hawaiite lavas have seriate to porphyritic textures (Fig. 2b). The most primitive lavas are olivine–phyric, and the modal abundance of clinopyroxene, Fe–Ti oxides and plagioclase phenocrysts gradually increases as the composition evolves. The petrology of the intermediate lavas (Fig. 2d) is characterized by a leucocratic groundmass surrounding abundant plagioclase phenocrysts (>50% throughout the intermediate suite). Euhedral clinopyroxene, olivine and oxide phenocrysts are ubiquitous in all potassic lava samples. Trachyte and phonolite lavas (Fig. 2f) are volumetrically minor at The Pleiades and occur as endogenous domes, such as Taygete Cone. They are classified as potassic by the absence of kaersutite, the presence of olivine microphenocrysts (0·1–0·3 mm) and their overall geochemical similarity to the intermediate lava compositions from the potassic lineage. Dominant phenocrysts are tabular sanidine with simple-twinning. Microphenocrysts (<0·7 mm) of green clinopyroxene and rounded olivine occur. The trachytic-textured groundmass is filled with feldspar-laths and interstitial clinopyroxene and oxides. Two trachyte samples

(M16012710 and M16012714-2) contain kaersutite pseudomorphs, but they differ from the evolved lavas of the sodic lineage in the presence of fayalitic olivine microphenocrysts.

Xenoliths and country rocks

The granodiorite xenoliths are clinopyroxene-bearing, hornblende–biotite granodiorite. They occasionally carry some cm- to mm-sized enclaves comprising hornblende and biotite. They show varying degrees of alteration, particularly of feldspar. Relatively fresh granodiorite xenolith samples (K16012407-2 and K16012422-3) were chosen for this study.

The two basement rocks collected around Terra Nova Bay are a migmatite and a deformed granite. The migmatite sample 141215-5B is a garnet–cordierite pelitic gneiss and its lithology is consistent with the description in Palmeri (1997). The granite sample 141123–1 A is representative of the GHIC group.

Mineral compositions

Olivine

Olivine shows a large compositional variation from Fo_{87} to Fo_{01}. In mafic lavas, euhedral olivine phenocrysts have a small variation in Fo content (Fo_{81} and $Fo_{84–87}$ in K16012424 and K16012708-4, respectively), whereas outermost rims or resorbed grains have a wider compositional range ($Fo_{68–86}$). Fayalite contents of olivine phenocrysts generally increase as the whole-rock wt % SiO_2 contents of their host lavas increase. Trachyte, the most evolved rock type in The Pleiades, contains nearly pure fayalite ($Fa_{98–99}$) microphenocrysts.

Clinopyroxene

Clinopyroxene is a ubiquitous phenocryst phase and shows variable compositions from diopside (or augite) to nearly pure hedenbergite. Because most of the clinopyroxene phenocrysts have sector, oscillatory and/or patchy zoning, their compositions vary widely, even within a single sample. However, the outer rims without disequilibrium textures show much narrower compositional variation. The rim compositions of clinopyroxene phenocrysts in basaltic rocks are moderately high in TiO_2 (1·2–4·3 wt %) and Al_2O_3 (4·2–9·2 wt %). Most of the clinopyroxenes have less than 0·1 atoms of Ti per 6 oxygens and are not titanian (Morimoto, 1988).

The clinopyroxene rim compositions in the mafic rocks are $Wo_{45–52}En_{34–44}Fs_{09–14}$ and become increasingly enriched in Fe ($Wo_{43–51}En_{29–41}Fs_{14–23}$) as the whole-rock composition evolves (Table 1). Clinopyroxene grains in trachyte and phonolite are strongly enriched in Fe ($Wo_{42–45}En_{02–24}Fs_{33–55}$) and do not overlap with other clinopyroxene compositional ranges in this study. Calculated Fe^{3+}/Fe^{2+} ratios ($Fe^{3+}=Na+{}^{IV}Al-{}^{VI}Al-2Ti-Cr$; Lindsley, 1983) of the trachytic clinopyroxene are restricted to a very low range (<0·1).

Amphibole

Amphibole phenocrysts are calcic, have high Ti contents (5·2–6·7 wt % TiO_2, 0·59–0·78 atom per formula unit, apfu; based on 24 oxygen per unit amphibole formula) and are pleochroic reddish brown in color. The high Ti content (Ti > 0·5 apfu) confirms the amphibole is kaersutite, a Ti- and Ca-rich oxy-amphibole (Hawthorne *et al.*, 2012). The Mg-numbers of the kaersutite phenocrysts do not vary significantly (Mg/[Mg+Fe+Mn]=0·5–0·7) among the lavas. However, iron-rich (Mg/[Mg+Fe+Mn]<0·5) kaersutite phenocrysts can be found as rounded cores or outermost rims.

Feldspar

The feldspar phenocrysts in the mafic to intermediate volcanic rocks are mainly plagioclase. The most mafic lavas do not contain plagioclase phenocrysts. The earliest plagioclase phenocrysts are 'labradorite' ($An_{66–60}$), although calcic (An_{80}) cores have been found. Throughout the mafic to intermediate lava compositions, the composition of plagioclase phenocrysts and microphenocrysts ranges from An_{80} to An_{30}.

Alkali-feldspar phenocrysts occur in the trachyte lavas. Some compositions cluster near the borderline between anorthoclase and sodian sanidine (Deer *et al.*, 2013). However, in this study, alkali-feldspars in trachyte and phonolite are simply called sanidine in accordance with the absence of albite and pericline twinning and the moderately potassium-rich ($Or_{>35}$) nature of most of the analysed alkali-feldspars.

Fe–Ti oxides and spinels

Fe–Ti oxides are ubiquitous except in the most mafic potassic lavas. Most of the oxide microphenocrysts are titanomagnetite. Their Fe^{2+}–Fe^{3+}–Ti compositions fall approximately in the middle of the ulvöspinel–magnetite solid solution line. Pure magnetite was found only as a sub-solidus exsolved phase in the titanomagnetite grains. Ilmenite is scarce and rarely coexists with titanomagnetite. Xenocrystic chrome-rich spinel, overgrown by titanomagnetite, can be found in some of the most mafic lavas.

Whole-rock compositions

Major elements

The volcanic rocks from The Pleiades exhibit a wide range of variation in alkali contents and in their degree of magmatic evolution (Table 2). The variation and classification are shown in the total alkalis vs silica (TAS) classification diagram (Fig. 3a) (Le Bas *et al.*, 1986). The sodic lineage lavas are basanite, tephrite, phonotephrite and tephriphonolite, whereas the potassic lineage consists of hawaiite, mugearite, benmoreite, trachyte and phonolite. The two lineages are identifiable on a K_2O vs Na_2O diagram (Fig. 3b). The sodic lineage has a slightly higher K_2O concentration than the potassic one in the mafic lavas and evolves to intermediate lavas with a constant Na_2O/K_2O ratio (~0·5). The potassic lineage

Table 1: Representative major element compositions of phenocrysts in The Pleiades volcanic rock samples

Sample	K1601 2424	K1601 2424	K1601 2424	K1601 2708-2	K1601 2708-2	K1601 2708-2	K1601 2708-2	K1601 2708-2	D1601 2403	D1601 2403	D1601 2403	D1601 2403	D1601 2403	K1601 2407-1	K1601 2407-1	K1601 2407-1	K1601 2407-1
Lineage	Potassic	Potassic	Potassic	Potassic	Potassic	Potassic	Potassic	Potassic	Potassic	Potassic	Potassic	Potassic	Potassic	Potassic	Potassic	Potassic	Potassic
Rock type	H	H	H	Mu	Mu	Mu	Mu	Mu	Bn	Bn	Bn	Bn	Bn	Tr	Tr	Tr	Tr
Mineral	Ol	Cpx	Mt	Ol	Cpx	Pl	Mt†	Ilm†	Ol	Cpx	Pl	Mt	Ilm	Ol	Cpx	Sa	Mt
SiO_2	39·37	48·69	0·15	36·93	50·06	55·51	0·14	0·02	35·15	49·52	56·38	0·08	0·17	29·44	49·43	67·15	0·18
TiO_2	b.d.l.	1·69	16·69	0·06	1·49	0·08	2·84	48·68	0·09	1·30	0·08	21·48	46·55	0·03	0·30	0·03	14·49
Al_2O_3	0·02	5·57	5·07	b.d.l.·	4·50	28·05	2·47	0·14	0·02	3·95	26·74	4·34	3·20	b·d·l·	0·44	19·14	0·07
Cr_2O_3	0·03	0·33	4·77	b.d.l.	b.d.l.	b.d.l.	0·06	b.d.l.	0·02	0·04	0·00	0·01	0·14	b·d·l·	25·03	0·01	b·d·l·
FeO	16·95	5·92	66·82	29·45	9·01	0·46	88·52	44·04	40·19	10·57	0·37	68·30	44·80	65·71	1·49	0·19	82·32
MnO	0·26	0·17	0·76	0·63	0·17	0·02	0·07	1·21	1·12	0·38	0·05	0·76	1·07	3·86	3·20	b·d·l·	1·08
MgO	43·07	14·15	5·09	32·65	13·32	0·02	1·07	3·88	23·59	12·42	0·05	2·88	2·44	0·78	18·97	b·d·l·	0·03
CaO	0·31	22·69	0·15	0·20	21·43	10·56	b.d.l.	b.d.l.·	0·27	20·92	9·42	b.d.l.	0·02	0·34	0·81	0·32	b·d·l·
Na_2O	0·02	0·41	0·01	b.d.l.	0·55	4·93	0·03	b.d.l.	0·07	0·67	5·87	0·04	0·02	b·d·l·	0·04	7·46	0·02
K_2O	b.d.l.	b.d.l.	0·04	b.d.l.	b.d.l.	0·47	0·01	0·01	0·01	0·02	0·56	0·01	0·01	b·d·l·	0·01	6·18	b·d·l·
NiO	0·12	b.d.l.	0·08	0·01	b.d.l.	b.d.l.	0·04	b.d.l.	b.d.l.	b.d.l.	b.d.l.	b.d.l.	0·08	b·d·l·	b·d·l·	b·d·l·	b·d·l·
Total	100·1	99·6	99·6	99·9	100·5	100·1	95·2	98·0	100·5	99·8	99·5	97·89	98·50	100·2	99·7	100·5	98·19
Mg#/An*	81·3	81·0		65·7	72·5	52·7			50·2	67·7	45·5			1·9	18·6		

Sample	K1601 2708-4	K1601 2708-4	K1601 2708-4	K1601 2708-4	K1601 2708-4	K1601 2708-4	K1601 2713-2	K1601 2713-2	K1601 2713-2	K1601 2713-2	K1601 2713-2	K1601 2422-2	K1601 2422-2	K1601 2422-2	K1601 2422-2	K1601 2422-2
Lineage	Sodic	Sodic	Sodic	Sodic	Sodic	Sodic	Sodic	Sodic	Sodic	Sodic	Sodic	Sodic	Sodic	Sodic	Sodic	Sodic
Rock	Bas	Bas	Bas	Bas	Bas	Bas	PhT	PhT	PhT	PhT	PhT	TPh	TPh	TPh	TPh	TPh
Mineral	Ol	Cpx	Krs	Pl	Mt	Ilm	Cpx	Krs	Pl	Mt	Mt	Cpx	Krs	Pl	Ne	Mt
SiO_2	40·38	47·56	39·02	51·61	0·10	0·05	47·42	38·56	55·55	0·09	0·08	44·94	38·25	59·41	45·04	0·02
TiO_2	0·01	2·28	6·47	0·12	17·97	48·07	1·88	6·64	0·09	19·64	0·58	2·50	5·63	0·04	b·d·l·	18·72
Al_2O_3	0·05	6·53	13·18	30·01	7·30	0·84	5·92	13·43	27·82	4·83	0·01	7·72	13·12	25·11	32·84	5·50
Cr_2O_3	0·06	0·16	0·04	b·d·l·	0·78	b·d·l·	0·01	b.d.l.	b.d.l.	0·04	b.d.l.	b.d.l.	0·02	b·d·l·	b·d·l·	b·d·l·
FeO	13·16	6·91	11·17	0·56	64·47	43·52	9·28	11·57	0·32	70·50	83·65	11·78	13·65	0·31	0·30	71·96
MnO	0·19	0·07	0·18	b.d.l.	0·45	0·48	0·22	0·11	0·03	0·70	0·01	0·33	0·10	b·d·l·	0·03	0·93
MgO	45·91	13·45	12·13	0·10	6·21	6·97	12·26	11·88	0·05	3·41	0·04	9·31	10·54	0·01	b·d·l·	2·18
CaO	0·29	21·63	11·73	13·14	b.d.l.	0·01	21·34	11·66	10·22	b.d.l.	b.d.l.	21·66	11·68	6·86	0·22	b·d·l·
Na_2O	b.d.l.	0·52	1·16	3·57	b.d.l.	b.d.l.	0·67	0·91	5·53	0·04	0·02	0·91	1·32	6·93	17·19	0·02
K_2O	b.d.l.	b.d.l.	2·49	0·31	b.d.l.	0·01	0·01	2·61	0·44	b.d.l.	0·02	0·03	2·48	0·82	3·96	b·d·l·
NiO	0·22	b.d.l.	b.d.l.	b.d.l.	b.d.l.	b.d.l.	b.d.l.	b.d.l.	b.d.l.	0·01	0·60	b.d.l.	b.d.l.	b·d·l·	b·d·l·	0·06
Total	100·3	99·1	97·6	99·4	97·3	99·9	99·0	97·4	100·0	99·3	85·0	99·2	96·8	99·5	99·6	99·4
Mg#/An*	85·6	77·6		65·8			70·2		49·2			58·5		33·7		

H, hawaiite; Mu, mugearite; Bn, benmoreite; Tr, trachyte; Bas, basanite; PhT, phonotephrite; TPh, tephriphonolite; Ilm, ilmenite; Ne, nepheline; b.d.l., below detection limit.
*Forsterite number, 100×Mg/[Mg+Fe+Mn+Ca], for olivine; Mg number, 100×Mg/[Mg+Fe] for clinopyroxene; anorthite number, 100×Ca/[Ca+Na+K] for plagioclase.
†A pair of exsolved and host phases of a single grain.

Table 2: Whole-rock major (wt %) and trace element (ppm) compositions of representative samples and the calculated CIPW normative mineral abundances

Group	P-M	P-M	P-M	P-M	P-M	P-I	P-I	P-I	P-I	P-I	P-I	P-I	P-I	P-I	P-I	P-F	P-F	P-F	P-F
Sample	K1601 2408-1	K1601 2424	J1412 0503-2	K1601 2408-2	M1601 2705-1	J1412 0504-4	K1601 2708-2	J1412 0106-1	D1601 2403	J1412 0105-1	J1412 0103	K1601 2708-1	K1601 2707-1	J1412 0504-1	K1601 2709-1	M1601 2701	K1601 2425	K1601 2415	K1601 2422-1
Rock type	AB	H	H	H	Bas	Mu	Mu	Mu	Bn	Bn	Bn	Tr	Tr	Tr	Ta	Ph	Ph	Ph	Tr
SiO_2	44·66	45·74	46·13	47·04	47·65	50·02	51·71	52·24	55·24	57·71	57·96	58·66	59·42	59·52	55·52	59·33	60·44	60·63	64·66
TiO_2	2·90	2·44	2·46	3·09	2·48	2·51	2·24	2·28	1·35	1·07	1·31	0·91	0·88	0·77	1·32	0·27	0·19	0·19	0·33
Al_2O_3	14·06	14·20	14·61	16·19	16·91	16·00	17·04	16·92	17·45	17·56	17·69	17·59	17·79	17·49	17·47	17·93	18·51	18·59	17·14
FeO_T	11·66	11·23	11·04	11·60	10·73	10·20	9·70	9·69	8·75	7·71	7·83	6·99	6·96	6·36	8·70	5·48	5·19	5·15	4·94
MnO	0·18	0·20	0·20	0·19	0·21	0·18	0·19	0·19	0·22	0·21	0·19	0·19	0·19	0·18	0·22	0·20	0·20	0·20	0·17
MgO	9·38	9·05	8·25	5·50	4·65	4·75	3·52	3·38	1·66	1·22	1·77	1·09	1·05	0·90	1·63	0·19	0·13	0·11	0·20
CaO	11·39	10·30	10·16	9·11	8·24	7·46	6·09	5·86	4·14	3·31	3·80	3·00	2·90	2·65	4·04	1·48	1·41	1·26	1·32
Na_2O	2·91	3·47	3·52	3·87	4·97	4·26	4·91	4·93	6·02	6·25	5·71	6·12	6·17	6·21	6·20	7·50	7·94	8·01	6·62
K_2O	1·32	1·42	1·48	1·73	2·07	2·35	2·77	2·78	3·53	3·90	3·81	4·29	4·37	4·45	3·52	5·43	5·48	5·50	5·30
P_2O_5	0·55	0·51	0·54	0·74	0·68	0·64	0·70	0·70	0·53	0·39	0·43	0·30	0·29	0·25	0·51	0·08	0·05	0·05	0·06
LOI	−0·12	0·05	0·00	−0·37	−0·47	0·00	0·14	0·00	−0·21	0·00	0·00	−0·25	−0·25	0·00	−0·20	0·00	0·13	0·03	−0·05
Total	98·89	98·61	98·37	98·69	98·12	98·37	99·00	98·96	98·67	99·35	100·5	98·89	99·78	98·78	98·94	97·89	99·67	99·73	100·7
ne	7·32	7·90	6·98	4·71	10·4	1·57	1·96	0·83	3·24	1·59		0·69	0·28		3·85	10·2	11·6	11·5	
di	25·7	23·6	22·4	15·5	15·6	12·6	7·82	7·21	5·85	4·71	3·83	4·36	3·87	4·11	6·16	6·14	5·94	5·24	4·14
ol	15·8	16·2	15·0	12·1	10·5	9·11	8·44	8·34	6·22	5·33	3·36	4·85	4·93	4·21	6·00	2·47	2·43	2·68	
hy											4·03			0·10					3·06
q																			1·76
Sc	35·6	25·7	n.d.	21·2	13·2	n.d.	11·2	n.d.	10·5	n.d.	n.d.	4·24	3·23	n.d.	7·33	1·07	0·65	0·87	2·51
V	303	227	n.d.	224	157	n.d.	124	n.d.	20·6	n.d.	n.d.	9·36	8·15	n.d.	18·1	1·98	0·91	1·85	0·60
Co	71·2	57·9	n.d.	47·6	37·3	n.d.	34·5	n.d.	23·9	n.d.	n.d.	13·7	12·4	n.d.	17·0	12·0	8·37	6·82	12·6
Cu	59·8	60·5	n.d.	47·2	35·5	n.d.	25·2	n.d.	29·0	n.d.	n.d.	9·09	9·01	n.d.	13·7	7·57	7·60	6·93	5·61
Rb	33·9	36·7	29·2	45·2	57·5	62·6	76·8	65·6	98·5	82·9	101	131	135	120	86·0	178	217	186	190
Sr	645	772	623	889	977	577	778	624	728	427·5	496	497	477	364	636	75·1	55·6	35·6	60·5
Y	27·5	27·0	21·7	27·6	30·5	23·7	30·8	25·5	41·7	30·6	28·1	32·2	33·1	26·9	37·1	33·0	38·9	32·7	41·8
Nb	70·7	82·2	58·9	82·4	121	77·0	118	84·5	164	116	109	158	159	117	150	120	219	163	192
Cs	0·41	0·52	0·61	0·75	0·84	1·56	1·13	1·29	1·57	1·55	1·94	2·34	2·55	2·35	1·55	3·60	3·82	3·76	5·08
Ba	391	608	547	565	876	524	791	689	1212	1130	907	1113	1126	1006	1171	752	340	282	610
Hf	5·39	5·36	5·21	5·47	6·91	7·34	8·32	8·06	10·8	11·1	11·7	12·3	12·9	12·5	10·1	14·9	18·3	15·3	15·6
Zr	220	224	184	235	343	281	386	334	572	465	483	605	643	553	484	807	936	809	748
Pb	2·24	2·64	2·51	3·23	4·11	7·22	7·80	6·73	8·47	9·26	10·3	13·3	11·9	12·3	7·41	9·45	16·2	12·4	13·7
Th	4·87	5·98	5·84	6·06	9·89	13·0	11·8	11·3	13·1	14·3	16·5	18·7	19·8	19·2	12·8	25·8	31·3	25·2	27·6
U	1·37	1·59	1·62	1·61	2·65	3·30	2·96	2·83	3·33	3·59	3·88	4·70	4·73	4·90	3·31	6·95	8·41	6·14	7·11
La	42·5	50·3	45·4	51·2	73·8	60·4	76·7	68·2	101	87·4	84·7	99·2	103	88·9	95·3	119	137	111	128
Ce	81·1	95·7	85·8	97·7	136	116	141	132	181	165	155	172	178	159	175	196	214	175	211
Pr	9·64	11·2	10·6	11·4	15·2	12·6	15·8	14·2	19·8	17·0	16·2	18·0	18·3	15·8	19·4	19·0	20·8	17·1	21·9
Nd	39·0	43·8	40·8	45·1	56·3	46·6	57·9	52·4	70·4	61·4	56·7	60·8	62·2	53·5	69·3	59·5	64·2	52·2	71·6
Sm	7·60	8·49	7·58	8·26	9·62	8·31	9·90	8·97	11·7	9·99	9·57	9·67	9·45	8·79	11·8	8·55	9·53	7·52	11·6
Eu	2·45	2·87	2·65	2·73	3·23	2·52	2·90	2·67	3·59	3·11	2·52	2·62	2·49	2·21	3·56	1·60	1·38	1·10	1·54
Gd	7·36	7·77	6·70	7·61	8·72	6·92	8·65	7·17	9·90	7·78	7·34	7·99	7·97	6·56	9·92	7·21	7·97	6·43	9·81
Tb	0·95	0·99	1·08	0·96	1·08	1·11	1·10	1·13	1·25	1·26	1·05	1·06	1·06	0·95	1·29	0·97	1·06	0·87	1·31
Dy	5·40	5·67	5·29	5·35	6·12	5·57	6·17	5·81	7·35	6·72	6·30	6·07	6·14	5·83	7·36	5·80	6·80	5·51	7·92
Ho	1·00	1·05	1·13	1·01	1·13	1·18	1·18	1·22	1·37	1·42	1·18	1·22	1·20	1·11	1·41	1·16	1·38	1·11	1·55
Er	2·61	2·77	2·70	2·68	3·08	2·93	3·33	3·06	3·86	3·66	3·35	3·56	3·58	3·23	4·02	3·52	4·30	3·43	4·64

(continued)

Table 2. Continued

Group	P-M	P-M	P-M	P-M	P-M	P-I	P-I	P-I	P-I	P-I	P-I	P-I	P-I	P-I	P-I	P-F	P-F	P-F	P-F
Sample	K1601 2408-1	K1601 2424	J1412 0503-2	K1601 2408-2	M1601 2705-1	J1412 0504-4	K1601 2708-2	J1412 0106-1	D1601 2403	J1412 0105-1	J1412 0103	K1601 2708-1	K1601 2707-1	J1412 0504-1	K1601 2709-1	M1601 2701	K1601 2425	K1601 2415	K1601 2422-1
Rock type	AB	H	H	H	Bas	Mu	Mu	Mu	Bn	Bn	Bn	Tr	Tr	Tr	Ta	Ph	Ph	Ph	Tr
Tm	0·35	0·36	0·38	0·35	0·40	0·43	0·44	0·45	0·54	0·55	0·51	0·52	0·51	0·51	0·54	0·54	0·66	0·55	0·68
Yb	2·12	2·29	2·20	2·19	2·63	2·57	2·89	2·74	3·53	3·45	3·28	3·45	3·53	3·31	3·60	3·69	4·69	3·79	4·77
Lu	0·31	0·31	0·37	0·32	0·37	0·43	0·43	0·45	0·52	0·57	0·52	0·52	0·53	0·53	0·52	0·57	0·69	0·58	0·69

Group	P-F	P-F	P-F	P-F	P-F	S-M	S-M	S-M	S-M	S-M	S-I	S-I	S-I	S-I	S-I	X	X	B	B
Sample	K1601 2407-1	J1412 0504-2	K1601 2412-1	M1601 2710	M1601 2714-2	K1601 2412-2	K1601 2411-1	J1412 0107-1	K1601 2708-4	K1601 2414	M1601 2707-1	M1601 2713-1	K1601 2713-2	K1601 2422-2	K1601 2713-1	K1601 2407-2	K1601 2422-3	1412 15-5B	1411 23-1A
Rock type	Tr	Tr	Tr	Tr (A)	Tr (A)	Bas	Bas	Tp	Bas	Bas	PhT	PhT	PhT	TPh	TPh	Gr·	Gr·	Mg	GHIC
SiO_2	64·73	64·93	66·01	60·27	61·04	43·97	43·98	44·84	45·62	47·12	48·23	48·46	50·41	53·03	54·89	67·44	68·85	59·24	69·17
TiO_2	0·28	0·47	0·25	0·62	0·63	3·56	3·65	2·99	3·29	2·60	2·55	2·29	2·04	1·23	1·08	0·61	0·58	1·04	0·45
Al_2O_3	16·40	17·78	16·45	18·33	18·54	14·53	14·82	15·56	14·81	16·30	17·32	17·52	17·45	19·11	18·65	14·64	14·81	16·46	16·30
FeO_T	4·92	4·85	4·72	5·18	5·26	11·88	11·87	11·20	11·04	11·29	10·54	9·86	9·97	8·10	8·26	3·56	3·25	8·93	3·10
MnO	0·18	0·16	0·16	0·19	0·19	0·19	0·19	0·21	0·18	0·21	0·23	0·22	0·21	0·24	0·22	0·07	0·06	0·31	0·06
MgO	0·13	0·51	0·06	0·57	0·60	7·14	6·45	5·07	7·29	5·84	3·44	3·00	2·97	1·26	1·46	2·15	1·95	4·77	1·14
CaO	1·15	1·74	1·08	2·12	2·11	10·90	10·76	9·68	9·60	8·91	7·66	7·06	6·19	4·59	4·17	3·20	3·32	0·99	4·20
Na_2O	6·63	6·19	6·72	6·77	6·70	3·42	3·58	4·64	3·68	4·80	5·80	6·24	5·85	7·47	6·80	3·87	3·92	1·28	4·02
K_2O	5·18	5·02	5·24	5·18	5·22	1·71	1·82	2·42	1·93	1·83	2·66	2·78	2·78	3·90	3·56	2·82	2·86	4·95	1·27
P_2O_5	0·05	0·15	0·03	0·14	0·15	0·68	0·72	0·82	0·56	0·63	0·62	0·55	0·68	0·36	0·50	0·05	0·05	0·05	0·07
LOI	−0·14	0·00	0·13	0·26	0·14	−0·62	−0·68	0·00	0·80	−0·27	−0·38	−0·24	−0·34	−0·20	−0·25	0·70	0·74	1·02	0·15
Total	99·52	101·8	100·8	99·62	100·6	97·37	97·16	97·43	98·80	99·26	98·68	97·74	98·21	99·09	99·33	99·11	100·4	99·02	99·93
ne				4·70	3·56	9·85	10·5	15·6	8·28	11·2	14·7	16·5	9·63	18·0	9·14				
di	4·79	1·48	4·54	4·52	3·75	25·1	24·7	23·7	21·3	18·5	17·1	16·7	11·0	11·4	6·47				
ol				2·79	3·15	11·5	10·3	8·34	12·7	11·8	5·26	4·48	6·79	3·01	5·51				
hy	2·82	4·82	2·72																
q	2·81	3·96	3·70																
Sc	3·97	n·d·	2·90	0·96	1·03	27·0	21·2	15·1	23·8	15·6	11·0	9·52	10·1	2·61	4·47				
V	1·45	n·d·	1·35	12·5	12·0	307	252	213	259	165	140	120	95·0	29·4	22·2				
Co	12·1	n·d·	9·46	12·1	12·1	58·1	48·8	44·2	51·5	46·2	33·4	28·6	30·5	14·1	21·8				
Cu	3·11	n·d·	7·09	7·00	6·04	57·3	43·4	40·5	46·4	42·6	29·5	24·1	23·2	9·52	12·3				
Rb	281	151	224	220	205	44·2	38·5	55·0	41·9	49·3	85·4	84·1	72·8	117	99·4				
Sr	39·6	199	7·47	419	382	842	729	822	828	883	1087	1020	1014	930	902				
Y	64·4	21·4	63·5	35·0	31·8	30·7	26·4	26·2	27·1	29·1	36·3	34·8	32·6	33·3	30·3				
Nb	291	116	184	140	147	89·1	77·8	105	86·9	106	152	135	137	197	166				
Cs	8·60	3·69	6·65	6·35	5·84	0·91	0·76	0·65	0·81	0·67	1·08	1·12	0·53	1·25	0·98				
Ba	377	705	70·3	1004	932	570	503	731	663	638	872	856	855	923	1032				
Hf	22·9	14·4	20·7	14·4	13·3	5·57	4·94	7·07	5·32	6·14	9·45	9·33	8·81	10·7	10·4				
Zr	1124	633	1016	785	724	232	204	285	222	280	490	509	455	565	559				
Pb	22·2	15·8	19·1	16·8	15·2	2·70	2·83	3·81	3·50	2·47	6·47	5·81	4·33	6·69	5·90				
Th	43·2	29·2	32·3	35·7	32·1	6·00	5·30	10·1	6·09	6·95	14·1	15·0	10·0	17·7	13·7				
U	10·7	7·36	8·01	10·5	8·66	1·63	1·43	2·61	1·63	1·91	3·80	4·12	2·59	4·77	3·19				

(continued)

Table 2. Continued

Group	P-F	P-F	P-F	P-F	P-F	S-M	S-M	S-M	S-M	S-M	S-I	S-I	S-I	S-I	S-I	X	X	B	B
Sample	K1601 2407-1	J1412 0504-2	K1601 2412-1	M1601 2710	M1601 2714-2	K1601 2412-2	K1601 2411-1	J1412 0107-1	K1601 2708-4	K1601 2414	M1601 2707-1	M1601 2713-1	K1601 2713-2	K1601 2422-2	K1601 2713-1	K1601 2407-2	K1601 2422-3	1412 15-5B	1411 23-1A
Rock type	Tr	Tr	Tr	Tr (A)	Tr (A)	Bas	Bas	Tp	Bas	Bas	PhT	PhT	PhT	TPh	TPh	Gr·	Gr·	Mg	GHIC
La	197	87·2	150	130	119	52·1	45·5	73·2	50·7	62·5	95·2	94·6	85·7	116	102				
Ce	328	148	265	212	193	101	88·6	141	98·5	117	173	167	153	199	174				
Pr	32·5	14·0	28·0	20·3	18·5	12·2	10·7	15·3	11·8	13·4	18·8	17·8	16·7	20·3	18·1				
Nd	104	44·0	95·2	64·3	58·0	49·4	43·4	58·4	46·9	50·7	68·4	64·2	60·5	67·8	60·7				
Sm	15·8	6·98	16·0	9·08	8·31	9·63	8·42	10·0	9·05	9·08	11·3	10·4	10·1	11·0	9·39				
Eu	1·25	1·37	0·95	2·03	1·88	3·05	2·66	3·18	2·89	2·87	3·56	3·29	3·20	3·13	2·95				
Gd	13·6	5·04	13·8	7·72	7·15	8·86	7·86	8·12	8·27	8·11	10·2	9·26	8·71	9·08	7·80				
Tb	1·84	0·75	1·89	1·01	0·92	1·11	0·98	1·27	1·03	1·04	1·27	1·16	1·08	1·12	0·95				
Dy	11·1	4·70	11·7	6·01	5·47	6·40	5·55	6·28	5·75	5·84	7·11	6·61	6·08	6·59	5·58				
Ho	2·23	0·89	2·30	1·19	1·09	1·16	1·00	1·29	1·07	1·08	1·34	1·25	1·14	1·22	1·05				
Er	6·55	2·67	6·79	3·64	3·31	3·03	2·62	3·16	2·84	2·94	3·73	3·45	3·11	3·53	2·97				
Tm	0·98	0·45	1·00	0·53	0·49	0·39	0·34	0·44	0·36	0·39	0·50	0·47	0·42	0·49	0·42				
Yb	6·57	2·99	6·84	3·75	3·40	2·43	2·10	2·64	2·24	2·48	3·25	3·14	2·68	3·34	2·80				
Lu	0·97	0·49	1·01	0·56	0·50	0·34	0·29	0·43	0·31	0·35	0·47	0·45	0·40	0·48	0·42				

P, Potassic; S, sodic; -M, mafic; -I, intermediate; -F, felsic; X, xenolith; B, basement rock; Gr., granodiorite; Mg, migmatite; Tr (A), amphibole-bearing trachyte; AB, alkali-basalt; Tp, tephrite; Ph, phonolite; n.d., not determined.

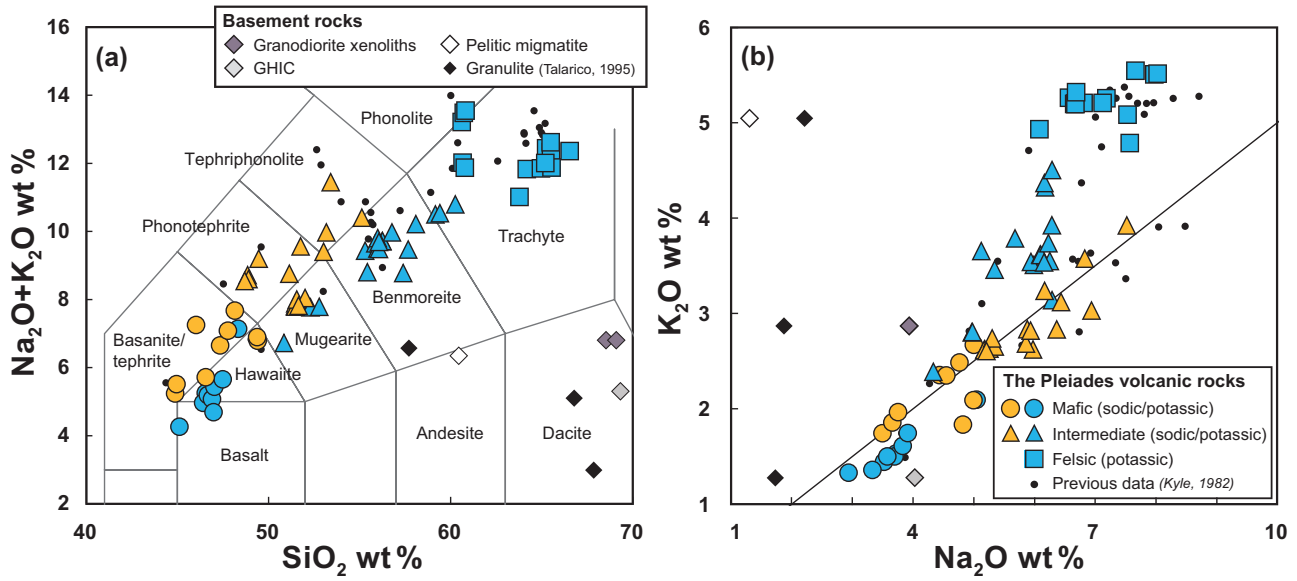

Fig. 3. Whole-rock chemical data for samples from this study. (a) Total alkalis vs silica (TAS) classification diagram for volcanic rocks from The Pleiades (Le Bas, 1986). Major element compositions are normalized to 100% anhydrous. The analysed AI xenoliths, pelitic migmatite and GHIC samples analysed in this study, together with previous Pleiades volcanic rock data (Kyle, 1982) and reported NVL relict granulite compositions (Talarico, 1995) are plotted for comparison. (b) A weight percent K_2O vs Na_2O diagram. The solid black line denotes $K_2O/Na_2O = 0{\cdot}5$.

diverges from the sodic lineage with increasing K_2O/Na_2O ratio (0·5–0·81). These two lithological groups fit the sodic and mildly-potassic lineages reported by Kyle (1982), implying a close relationship between geochemical divergences and fractionating phases.

The variations of the major element lava compositions are plotted in Fig. 4. Although both lineages follow similar trends of sharp decreases in MgO, FeO_t, CaO and TiO_2 and increases of Al_2O_3, Na_2O and K_2O in the mafic suites with increasing SiO_2, the basanites of the sodic lineage tends to have slightly more TiO_2, Al_2O_3, Na_2O, K_2O and P_2O_5 and less MgO and CaO than hawaiite in the potassic lineage. Among the intermediate lavas, the sodic lineage is characterized by stronger depletion of TiO_2, FeO_t, MgO and P_2O_5 and by higher contents of Al_2O_3, Na_2O and K_2O than the potassic lineage. It is also notable that there is a sharp shift in the trend from the mafic to intermediate lava compositions in the potassic lineage for Al_2O_3 and Na_2O, whose increasing trends flatten or even decrease with increasing SiO_2.

As mentioned above, all felsic rocks are grouped as the potassic lineage based on the absence of kaersutite and presence of olivine. Indeed, the plateau of high K_2O concentrations (4·8–5·5 wt %) with respect to Na_2O supports the idea that the felsic lavas, even in the case of phonolite, are linked to the potassic lineage rather than the sodic one. The trachyte samples are characterized by their highly depleted TiO_2 (<0·6 wt %), CaO (<2·1 wt %), MgO (<0·6 wt %), FeO_t (<5·5 wt %) and P_2O_5 (<0·15 wt %) contents and by high K_2O (>4·3 wt %) contents. A gap in SiO_2 contents (61·0–64·2 wt %), accompanied by a slight drop in Al_2O_3 from the benmoreite to the trachyte samples, is also notable. The phonolite, on the other hand, becomes more enriched in Al_2O_3 and slightly more alkali enriched than the trachyte samples, without a significant SiO_2 increase.

The two granodiorite xenoliths plot in the andesite field in the TAS diagram, and their compositions are slightly alkali-rich compared to those of the GHIC sample (141123-1A; Fig. 3). The cordierite garnet migmatite sample (141215-5B) is less silica-rich, deficient in Na_2O (1·3 wt %), and enriched in K_2O (5 wt %).

Trace elements

Selected trace element variations in The Pleiades volcanic rocks are plotted in Fig. 5. Mafic to intermediate rocks from both lineages share common trends of positive correlations between SiO_2 content and REE abundances, high field strength elements (HFSE), alkali elements (Cs and Rb), Ba, and Pb. Transition metals Sc, V, and Cu, sharply decrease before SiO_2 contents reach 50 wt % and then gently decrease in more evolved rocks. However, it should be noted that the mafic sodic lineage is characterized by slightly higher contents of large ion lithophile elements (LILE), Nb, light-REE (LREE), and middle-REE (MREE) and lower contents of transition metals (except V) than the mafic potassic lineage. The discrepancy becomes larger in the intermediate rocks. The decreasing trends of the MREE, Eu, and Gd, are distinct from the gently increasing trends of the potassic lineage. The intermediate sodic lavas are also marked by their high Sr concentrations (>800 ppm) relative to the other samples studied,

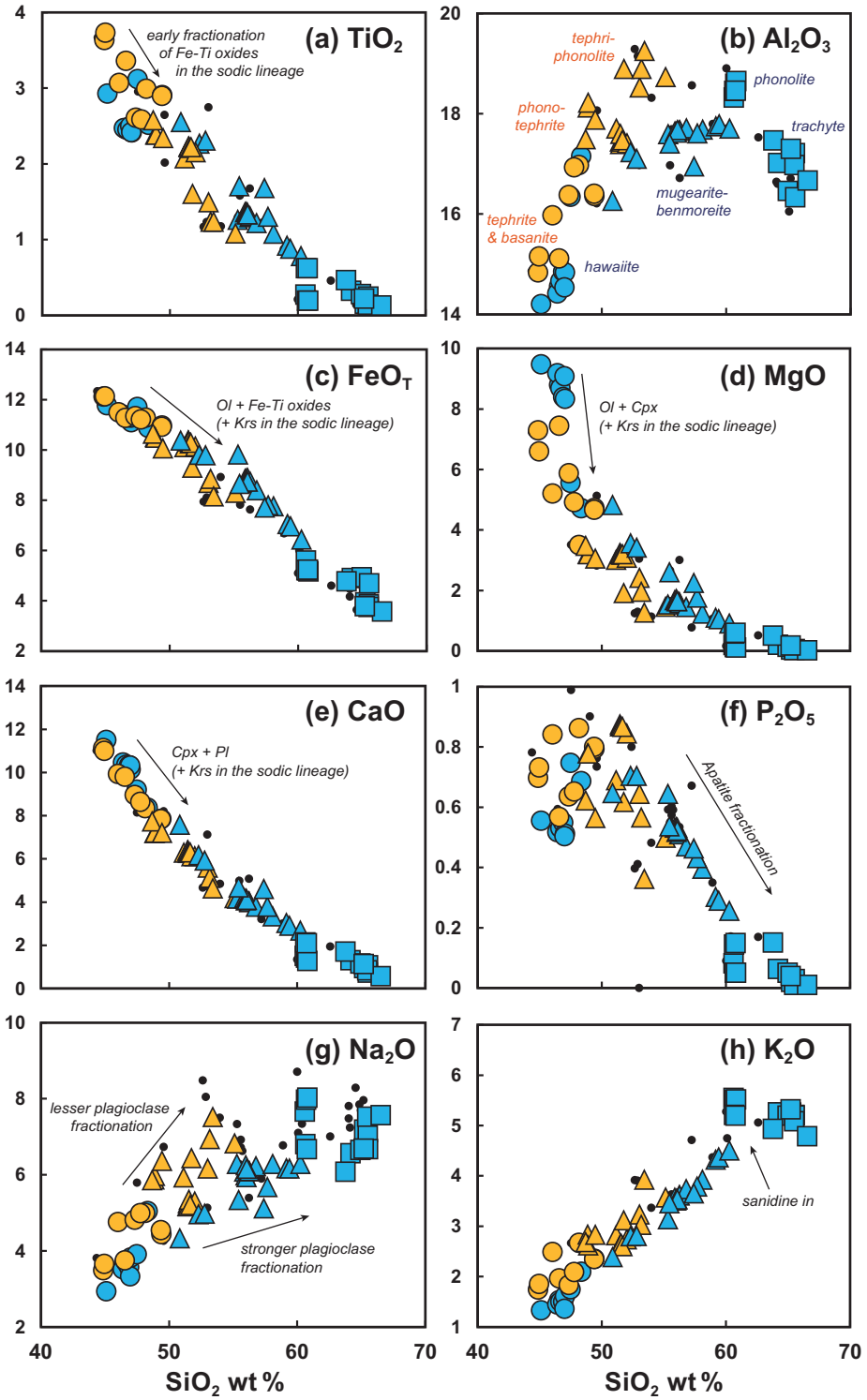

Fig. 4. Whole-rock Harker diagrams for The Pleiades lava samples (this study and Kyle, 1982; in wt %). See Fig. 3 for symbol definitions.

whereas the Sr content in the potassic lineage decreases from ~ 1000 ppm to below 800 ppm as their SiO_2 exceeds 50 wt %.

The trace element variations in trachyte and phonolite are marked by extreme enrichments or depletions. Concentrations of transition metals and the feldspar-hosted elements Sr, Ba and Eu decrease to almost zero, whereas the concentrations of other incompatible trace elements such as Zr increase. Barium concentration increases in both lineages up to 1270 ppm in the intermediate rocks, but then decreases in the trachyte samples.

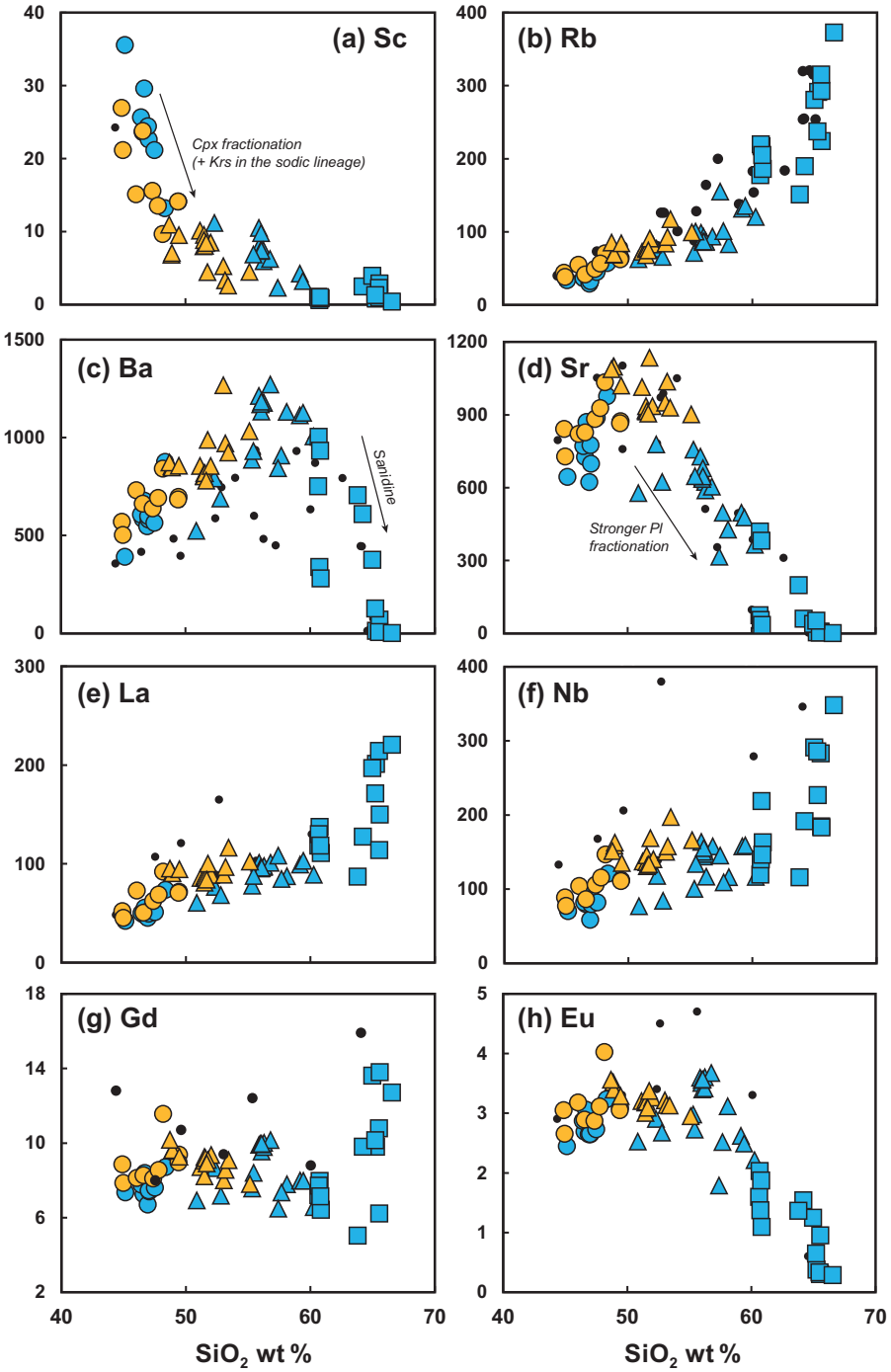

Fig. 5. Silica variation diagrams showing selected trace elements (in ppm) for The Pleiades lava samples. See Fig. 3 for symbol definitions.

Primitive mantle normalized trace element patterns are plotted in Fig. 6. The mafic rocks from the two lineages share the same OIB-like intraplate volcanic patterns with enrichment in highly to moderately incompatible trace elements. All samples show highly fractionated patterns with negative K and Pb anomalies, mild Th, U, Zr, Hf troughs and positive Nb anomalies.

Different behavior of Sr between the intermediate sodic and potassic lineages is evident in Fig. 6c and d. The evolved lavas of both lineages share concave upward patterns in the middle- to heavy-REE. Extreme enrichment of most elements compared to mafic lavas and strong depletion of Ba, Sr and Eu in trachyte and phonolite lavas are prominent in Fig. 6e.

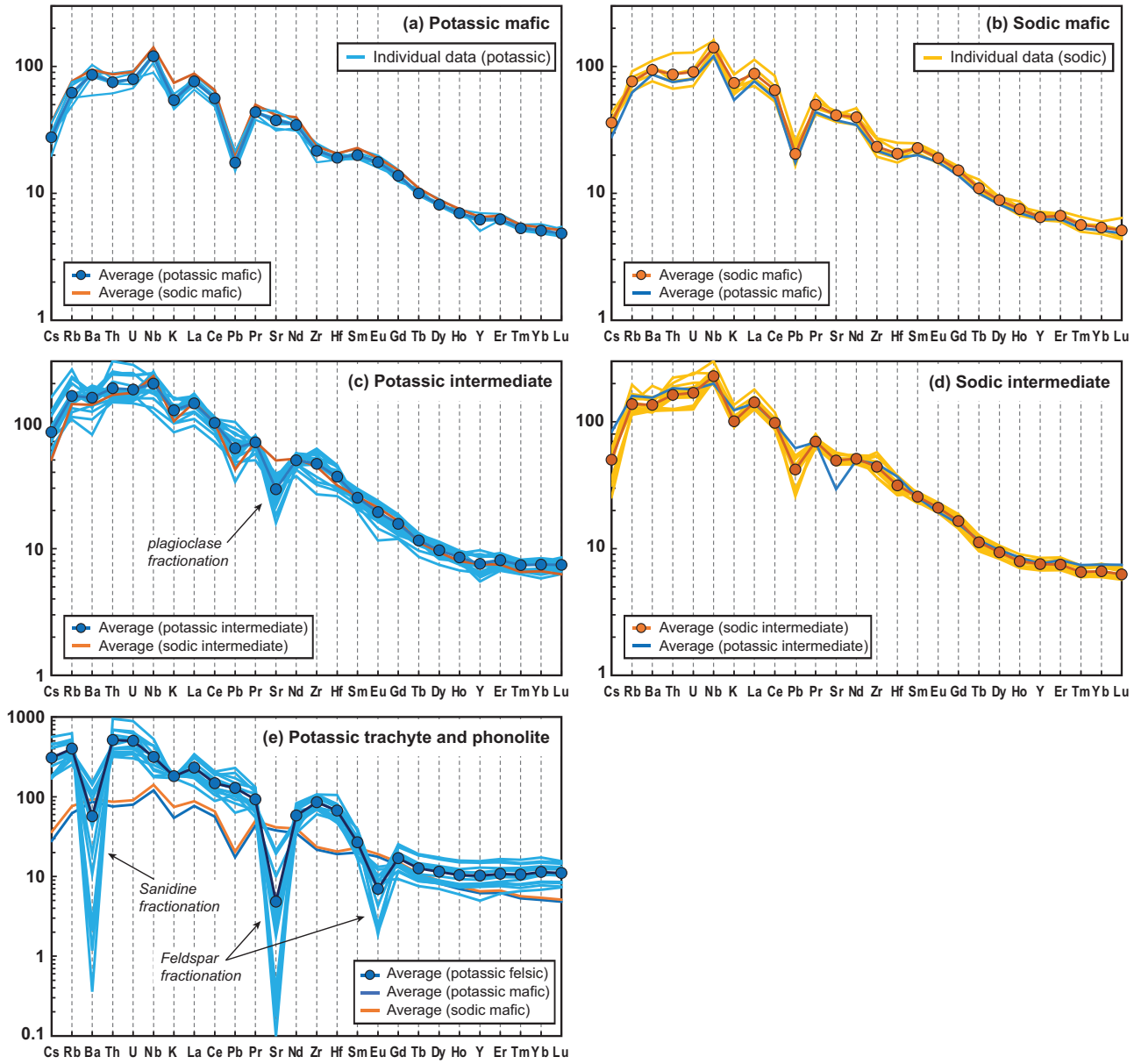

Fig. 6. Whole-rock primitive mantle normalized (McDonough & Sun, 1995) trace element patterns for The Pleiades volcanic rocks. (a–d) The averaged values and the average compositions from their counterpart lineage are shown together. In (a) and (b), mafic rocks with MgO less than 5 wt % are excluded. (e) Trachyte and phonolite compositions are plotted together with the average mafic lava compositions from (a) and (b) for comparison.

Sr–Nd–Pb isotopes

Volcanic rocks

Whole-rock Sr, Nd, and Pb isotopic compositions have been measured on six sodic lineage and twelve potassic lineage samples (Table 3; Fig. 7). The sodic lineage lavas have a narrow range in $^{87}Sr/^{86}Sr$ and $^{143}Nd/^{144}Nd$ from 0·703143 to 0·703442 and 0·512859 to 0·512897 (ε_{Nd} = 4·3–5·1), respectively. Lead isotopes also have narrow ranges of $^{206}Pb/^{204}Pb$ (19·7–19·9), $^{208}Pb/^{204}Pb$ (39·5–39·6) and $^{207}Pb/^{204}Pb$ (15·6), except for an outliner, K16012708-4, whose Pb isotopic ratios are $^{206}Pb/^{204}Pb$ (19·4), $^{208}Pb/^{204}Pb$ (39·3) and $^{207}Pb/^{204}Pb$ (15·6) (Fig. 7c and d). None of those isotopic ratios from the sodic lineage correlates with differentiation indices such as SiO_2, MgO or Th.

The potassic lineage shows wider variation in Sr, Nd, and Pb isotopic ratios than the sodic lineage. The mafic potassic samples are similar in isotopic composition to those of the sodic lineage, whereas the evolved (SiO_2>50 wt %) samples have more elevated $^{87}Sr/^{86}Sr$ (>0.70370) and lower $^{143}Nd/^{144}Nd$ (<0·51280), $^{206}Pb/^{204}Pb$ (<19·5) and $^{208}Pb/^{204}Pb$ (<39·4). Unlike other mafic potassic samples, one sample (K16012408-1) has high $^{87}Sr/^{86}Sr$ (0·704003) and low $^{143}Nd/^{144}Nd$ (0·512797).

The isotopic compositions of the mafic rocks from The Pleiades generally overlap with primitive lavas from Mt. Melbourne (Lee *et al.*, 2015), Mt. Erebus, and Mt. Morning (Sims *et al.*, 2008; Martin *et al.*, 2013). In Fig. 7, the Sr–Nd–Pb isotope data for the Ross seafloor

Table 3: Whole-rock Sr, Nd and Pb isotopic compositions of The Pleiades samples

Sample	Group	Rock type	$^{87}Sr/^{86}Sr$	$\pm2\sigma$ ($\cdot10^{-6}$)	$^{143}Nd/^{144}Nd$	$\pm2\sigma$ ($\cdot10^{-6}$)	$^{206}Pb/^{204}Pb$	$\pm2\sigma$ ($\cdot10^{-4}$)	$^{207}Pb/^{204}Pb$	$\pm2\sigma$ ($\cdot10^{-4}$)	$^{208}Pb/^{204}Pb$	$\pm2\sigma$ ($\cdot10^{-4}$)
K16012408-1	P-M	AB	0·704003	5	0·512797	6	19·051	17	15·639	16	39·094	49
K16012424	P-M	H	0·703232	5	0·512876	4	19·641	9	15·624	8	39·484	26
J14120503-2	P-M	H	0·703272	5	0·512831	10	19·598	9	15·628	8	39·476	25
J14120504-4	P-I	Mu	0·703717	5	0·512813	6	19·159	6	15·638	5	39·143	16
J14120106-1	P-I	Mu	0·704027	5	0·512781	7	19·072	6	15·636	6	39·095	18
J14120107-2	P-I	Bn	0·703477	5	0·512847	5	n.d.		n.d.·		n.d.	
J14120105-1	P-I	Bn	0·703884	5	0·512805	6	19·195	10	15·640	9	39·198	28
J14120103	P-I	Bn	0·703998	5	0·512791	6	19·056	8	15·638	7	39·093	22
J14120504-1	P-I	Tr	0·703999	5	0·512797	5	19·052	8	15·640	7	39·094	23
K16012709-1	P-I	Bn	0·703852	5	0·512823	7	19·205	8	15·635	8	39·188	24
K16012425	P-F	Ph	0·703973	5	0·512813	6	19·510	14	15·636	12	39·425	38
M16012710	P-F	Tr	0·703747	5	0·512811	5	19·229	7	15·641	6	39·245	19
J14120107-1	S-M	Tp	0·703143	6	0·512872	7	19·721	9	15·625	8	39·524	26
K16012708-4	S-M	Bas	0·703442	6	0·512870	5	19·371	7	15·642	7	39·300	21
M16012713-1	S-I	PhT	0·703182	5	0·512880	6	19·993	8	15·656	7	39·781	23
K16012713-2	S-I	PhT	0·703169	5	0·512859	9	19·849	9	15·629	8	39·630	24
K16012422-2	S-I	TPh	0·703190	6	0·512897	8	19·772	8	15·631	7	39·568	21
K16012713-1	S-I	TPh	0·703152	5	0·512891	4	19·856	8	15·627	7	39·632	24
K16012407-2	X	Gr·	0·715561	5	0·512387	6	18·966	10	15·660	9	39·139	28
K16012422-3	X	Gr·	0·715740	5	0·512356	4	18·552	6	15·632	5	39·013	17
141215-5B	B	Mg	0·761940	5	0·511751	4	18·203	6	15·687	5	39·040	17
141123-1A	B	GHIC	0·714313	4	0·511908	6	18·197	4	15·647	4	38·482	11

P, potassic lineage; S, sodic lineage; -M, mafic; -I, intermediate; -F, felsic; X, xenolith; B, basement rock; AB, alkali-basalt; H, hawaiite; Mu, mugearite, Bn, benmoreite; Tr, trachyte; Ph, phonolite; Tp, tephrite; Bas, basanite; PhT, phonotephrite; TPh, tephriphonolite; Gr·, Al granodiorite; Mg, migmatite; GHIC, Granite Harbour Intrusive Complex; n.d., not determined.

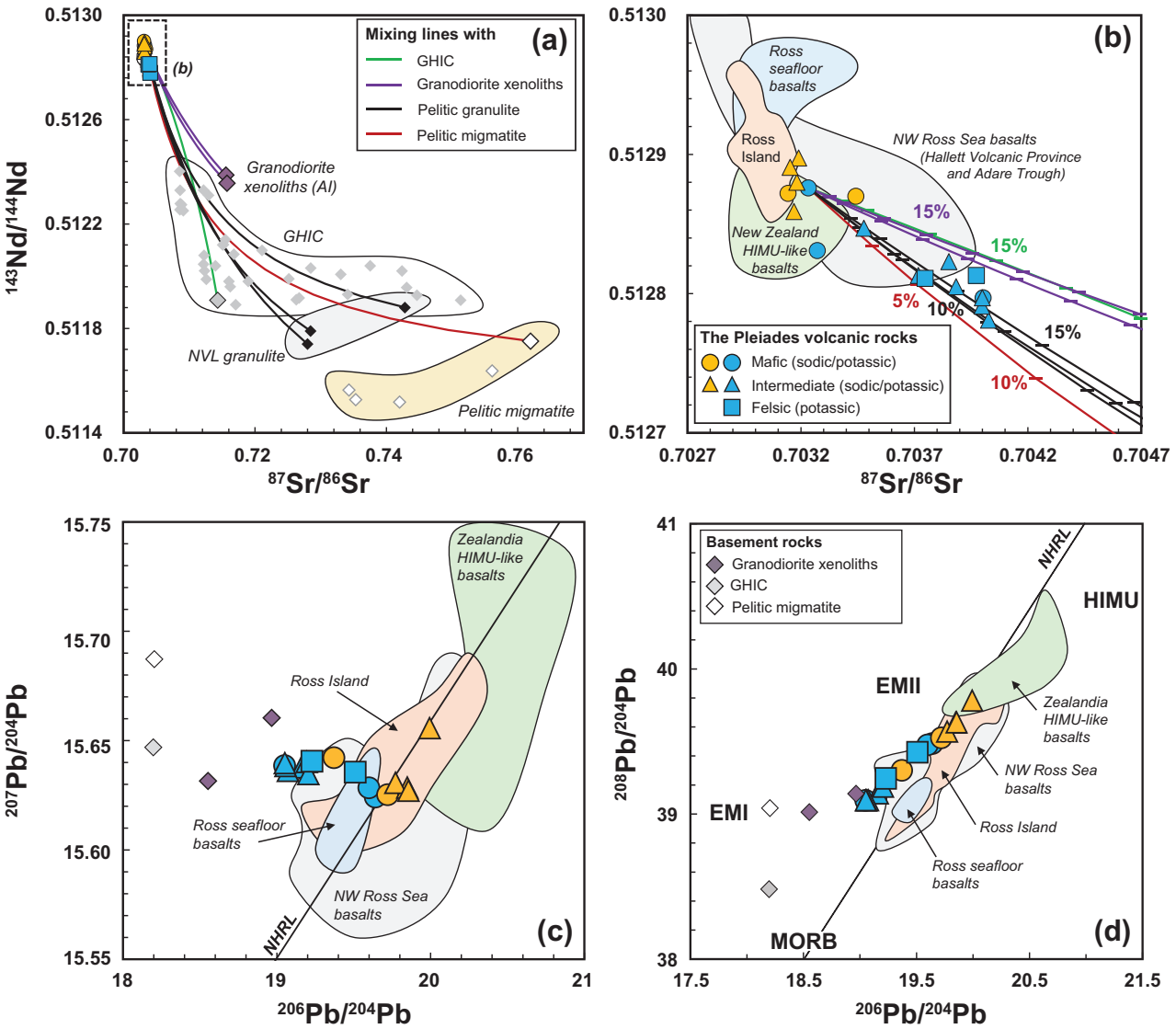

Fig. 7. (a), (b) $^{143}Nd/^{144}Nd$ vs $^{87}Sr/^{86}Sr$ and (c) $^{207}Pb/^{204}Pb$ and (d) $^{208}Pb/^{204}Pb$ vs $^{206}Pb/^{204}Pb$ for The Pleiades volcanic rocks and analysed basement rocks. Basement rock data include: Northern Victoria Land (NVL) granulite (Talarico, 1995), GHIC granitoids (Armienti *et al.*, 1990; Di Vincenzo & Rocchi, 1999; Dallai *et al.*, 2003); the pelitic migmatite (Di Vincenzo *et al.*, 1999). Also plotted are young alkali-rich basalts from the northwest Ross Sea (Panter *et al.*, 2018), Zealandia (Panter *et al.*, 2006) and the Ross seafloor (Lee *et al.*, 2015). Mixing lines are shown between the mafic potassic lava sample (J14120503-2) and potential contaminants (GHIC, granodiorite Al xenoliths, granulite, and migmatite). End-member mantle components in (d) are from Zindler & Hart (1986).

basanite (Lee *et al.*, 2015), the northwest Ross Sea basalts (mostly the Adare Trough and the Hallett Volcanic Province lavas; Panter *et al.*, 2018), and the New Zealand HIMU-like basalts (Panter *et al.*, 2006) are plotted together to illustrate that the isotopic ratios of the most mafic suites in The Pleiades are comparable with the isotopic range of those basaltic rocks.

Basement rocks

The granodiorite xenoliths from The Pleiades have elevated $^{143}Nd/^{144}Nd$ (0·512356 and 0·512387) compared to the migmatite and the GHIC samples (0·511751 and 0·511908, respectively; Fig. 7a). The $^{87}Sr/^{86}Sr$ of the migmatite sample (0·761940) is much higher than that of the xenoliths (0·715561 and 0·715740) and the GHIC (0·714313). The $^{206}Pb/^{204}Pb$ ratios of the GHIC and migmatite (both are 18·20) are much less than the granodiorite xenoliths (18·55 and 18·97). Although $^{143}Nd/^{144}Nd$ is slightly high, the isotopic ratios of the GHIC sample are broadly similar to reported data on the GHIC (Armienti *et al.*, 1990). The isotopic ratios of the granodiorite xenoliths are distinct from both GHIC (Armienti *et al.*, 1990; Di Vincenzo & Rocchi, 1999; Dallai *et al.*, 2003) and Al (Borg *et al.*, 1987; Armienti *et al.*, 1990).

DISCUSSION

Pressure and temperature

Phenocryst compositions and crystallization in magmas are controlled by pressure (depth) and temperature

Table 4: Liquidus pressure and temperature estimated using the thermobarometers described in Putirka *et al.* (2003), Putirka (2008) and Masotta *et al.* (2013)

Sample	Group	n	Putirka *et al.* (2003)				Putirka (2008)				Masotta *et al.* (2013)			
			T (°C)	±1σ	P (kbar)	±1σ	T (°C)	±1σ	P (kbar)	±1σ	T (°C)	±1σ	P (kbar)	±1σ
K16012424	P-M	10	1227	5·9	11·1	0·5	1202	8·4	11·4	0·6				
K16012424 (R)*	P-M	4	1195	3·3	9·4	0·3	1192	2·4	10·1	0·5				
K16012408-2	P-M	5	1173	3·3	9·5	0·3	1185	6·1	12·0	0·3				
M16012705-1	P-M	2	1133		8·3		1158		10·7					
K16012708-2	P-I	5	1081	2·5	6·9	0·4	1090	4·7	9·9	0·5				
K16012708-2 (R)	P-I	1	1131		7·5		1131		10·2					
K16012412-1	P-F	6									853	7·4	1·0	0·3
K16012407-1	P-F	2									859		1·5	
K16012708-4	S-M	2	1195		10·1		1174		11·5					
K16012708-4 (R)	S-M	6	1150	4·0	8·2	0·3	1163	3·5	10·0	0·6				
K16012414	S-M	2	1167		9·9		1174		11·8					
M16012707-1	S-I	7	1094	3·4	7·9	0·3	1121	5·6	11·3	0·3				
K16012713-2	S-I	2	1064		7·1		1086		10·2					

*(R) denotes the re-equilibrated calculation. The re-equilibrated whole-rock compositions of K16012424, K16012708–2 and K16012708–4 are those of K16012412-2, J14120504–4 and J14120107–1, respectively. Refer to Supplementary Data for the result of each clinopyroxene-liquid pair.

conditions during their ascent through the crust (e.g. Ablay *et al.*, 1998; Genske *et al.*, 2012; Grant *et al.*, 2013; Putirka, 2017). Clinopyroxene–melt thermobarometry (Putirka *et al.*, 2003; Putirka, 2008) is used here to estimate liquidus temperatures and pressures. Clinopyroxene is ubiquitous in all the lavas. The core textures and compositions of clinopyroxene in The Pleiades volcanic rocks are variable, but the cores are mostly enveloped by euhedral outer rims with a more restricted range of composition, implying there was equilibrium with the surrounding melt composition during the last stage of magma evolution before the eruption.

Rim compositions of clinopyroxene phenocrysts without disequilibrium textures were used for the calculations. Phenocrysts with fine oscillatory zoning and sector zoning were excluded. The whole-rock compositions of samples containing $< 5\%$ total phenocryst area in thin section were used for liquid compositions, because neither co-existing melt inclusions nor glassy lavas were available. The whole-rock composition, however, does not necessarily equilibrate with the clinopyroxene rim compositions (e.g. Giacomoni *et al.*, 2016). Putirka (2008) suggested that the equilibrated pairs of liquid and clinopyroxene produce a specific range of $K_D(Fe–Mg)^{Cpx\text{-}liquid} = 0{\cdot}28 \pm 0{\cdot}08$ which is slightly temperature dependent. We used the clinopyroxene–whole-rock pairs whose $K_D(Fe–Mg)^{Cpx\text{-}liquid}$ values fall within the 20% of equilibrium values using equation 35 from Putirka (2008). If clinopyroxene rim compositions were out of equilibrium with their host, then the paired whole-rock compositions were replaced by another of The Pleiades lava compositions which produced the appropriate equilibrium K_D value (e.g. Giacomoni *et al.*, 2016). The clinopyroxene compositions which fail to be equilibrated after this correction were considered to be xenocrysts and excluded from the data and discussion.

Temperatures and pressures were calculated for the selected clinopyroxene–liquid pairs using the clinopyroxene–liquid thermobarometer from Putirka (2008). Equations 31 and 33 were used and give values with standard errors of ± 2·9 kbar and ± 45°C. The amounts of H_2O in the potassic and sodic lavas in The Pleiades were assumed to be 0·5 wt % and 1·5 wt %, respectively, based on melt inclusion data from Ross Island whose two representative fractionation trends (DVDP and Erebus lineages) resemble those of The Pleiades (Rasmussen *et al.*, 2017). It should be noted that a change of ± 1 wt % H_2O produces only about ±0·4 kbar difference, which is within the error of the calculated values.

The results of the thermobarometry are shown in Table 4 and Fig. 8. The mafic samples (K16012424, K16012408-2, M16012705-1, K16012708-4, and K16012414) record higher temperatures (1152–1216°C) than the intermediate ones (K16012708-2, M16012707-1, and K16012713-2; 1082–1130°C). Although the calculated pressure ranges for the mafic and intermediate lavas broadly overlap, mafic lavas record higher pressure (10·1–12·5 kbar) than the intermediate lavas (9·1–11·7 kbar). The 're-equilibrated' clinopyroxene–liquid pairs from the mafic lavas also produce a similar temperature range (1156–1196°C), but show slightly lower pressure conditions (9·3–10·9 kbar) similar to the range of the intermediate lavas.

The K_D values between the trachyte whole-rock and clinopyroxene phenocrysts (excluding aegirine-augite) vary widely from 0·14 to 0·29. Among them, seven grains are within the expected equilibrium range based on the Putirka (2008) equation 35. The calculated pressure and temperature conditions are much lower (841–864°C, 0·8–1·7 kbar), broadly consistent with previous plagioclase thermometry estimates (776–891°C; Kyle, 1986). Masotta *et al.* (2013) provided a modified K_D equation (Equation 35alk) specifically for the trachyte–phonolite system. According to this modified equation, one clinopyroxene–whole-rock pair is at equilibrium

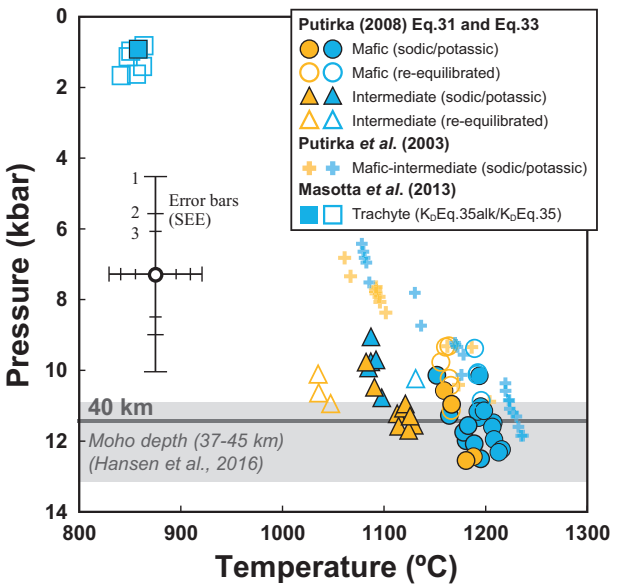

Fig. 8. Calculated pressure and temperature conditions of The Pleiades volcanic rocks based on the clinopyroxene-liquid thermobarometry. The equations from Putirka *et al.* (2003) and Equations 31 and 33 from Putirka (2008) were used for the mafic to intermediate lavas. Open circles are the estimated values from the re-equilibrated clinopyroxene–liquid pairs; open squares are the clinopyroxene–liquid pairs which are within the equilibrium range based on the Equation 35 in Putirka (2008); the filled square is the estimated pressure and temperature based on the methods described in Masotta *et al.* (2013). The grey bar is the equivalent pressure range of the reported Moho depths (Hansen *et al.*, 2016) assuming the mean crustal density is 3·0 g/cm^3. The error bars denote standard error of estimates (SEE) of 45°C and 2·9 kbar (number 1) for Putirka (2008), 33°C and 1·7 kbar (number 2) for Putirka *et al.* (2003), and 18·2°C and 1·15 kbar (number 3) for Masotta (2013) methods.

and produces similar crystallization conditions (858°C, 0·9 kbar). Therefore, crystallization of clinopyroxene in the trachyte lavas occurred at a very shallow depth (<2 kbar) and low temperature (~ 850°C).

The Moho depth below the TAM in NVL has been estimated to be about 40 km (Block *et al.*, 2009; Hansen *et al.*, 2016), which is similar to Southern Victoria Land (e.g. Bannister *et al.*, 2003; Lawrence *et al.*, 2006; Watson *et al.*, 2006; Chaput *et al.*, 2014). The 40 km depth is equivalent to a pressure of 11–12 kbar, assuming a crustal density of 2·8–3·1 g/cm^3. The crystallization pressures of 10·1–12·5 kbar, estimated from the mafic lavas of The Pleiades, indicate the mafic magmas crystallizing at the Moho. Crystallization pressures for the intermediate composition lavas (6·4–11·7 kbar) fall in the range of lower crustal pressures (Fig. 8). The above calculation suggests that the mafic to intermediate lavas of The Pleiades have mainly pooled at the Moho and in the lower crust.

The calculations from the trachyte samples record much shallower depths (<2 kbar). The shallow emplacement of felsic magmas is consistent with other trachyte and phonolite studies (Peccerillo *et al.*, 2007; Martel *et al.*, 2013; Moussallam *et al.*, 2013; Brenna *et al.*, 2015). The low pressure conditions may indicate a shallow magma chamber (Brenna *et al.*, 2015) or conduit-fill, endogenous dome or cryptodome emplacement (Hoblitt & Harmon, 1993; Hammer *et al.*, 1999). Endogenous dome emplacement is recorded at Taygete Cone. In whichever case, the vesicle-poor and crystal-rich features of trachyte are consistent with shallow-depth degassing processes.

It is notable that the mafic and intermediate magmas of the two lineages share similar liquidus pressure and temperature ranges. Some lavas exhibit mingling textures of kaersutite-bearing and plagioclase-rich melts. This suggests that the mixing of the two lineages may have occurred in the lower crust. Therefore, the evolution of the two lineages should be attributed to factors other than pressure and temperature conditions, because the two lineages have similar crystallization conditions at lower crustal depths.

Effect of fractional crystallization

The sodic and potassic fractionation trends

The systematic difference in chemical composition between the two lithological groups can be explained by fractional crystallization processes. Least-squares mass-balance models (OPTIMASBA software; Cabero *et al.*, 2012) were calculated using the measured whole-rock and crystal compositions (Fig. 9). Representative whole-rock compositions used for the parent and daughter magma compositions and the measured phenocryst compositions of the parent stage used for fractionating crystal compositions are reported in Table 5. In order to investigate the potential effect of crustal contamination processes, the whole-rock compositions of the migmatite sample, the GHIC and the granodiorite AI xenolith samples, and granulite data from Talarico *et al.* (1995) were included in the model. All calculations produced good regression fits (R^2>99·99%; SEE ≤ 0·10).

The results of the mass balance model are consistent with petrography, showing that the compositional variation of the sodic lineage is mainly controlled by clinopyroxene and kaersutite fractionation. The removal of about 45 wt % of crystalline solid with the assemblage olivine (8, i.e. 8% of the crystalline solid), clinopyroxene (33), kaersutite (36), plagioclase (15), Fe–Ti oxides (7), and apatite (1) can explain the trend from hawaiite (K16012708-4, MgO = 7·3 wt %) to phonotephrite (K16012713-2, MgO = 3·0 wt %) (trend S1 in Fig. 9). Although kaersutite is one of two alkali-rich phases together with plagioclase, fractionation of kaersutite suppresses the fractionation of olivine and plagioclase, which results in the alkali-rich nature of the sodic lineage.

The compositional variation from phonotephrite (K16012713-2, SiO_2=51·2 wt %) to tephriphonolite (K16012713-1, SiO_2=55·1 wt %) in the sodic lineage (trend S2, Fig. 9) can be produced by 28 wt % fractionation of kaersutite (36), clinopyroxene (21), plagioclase

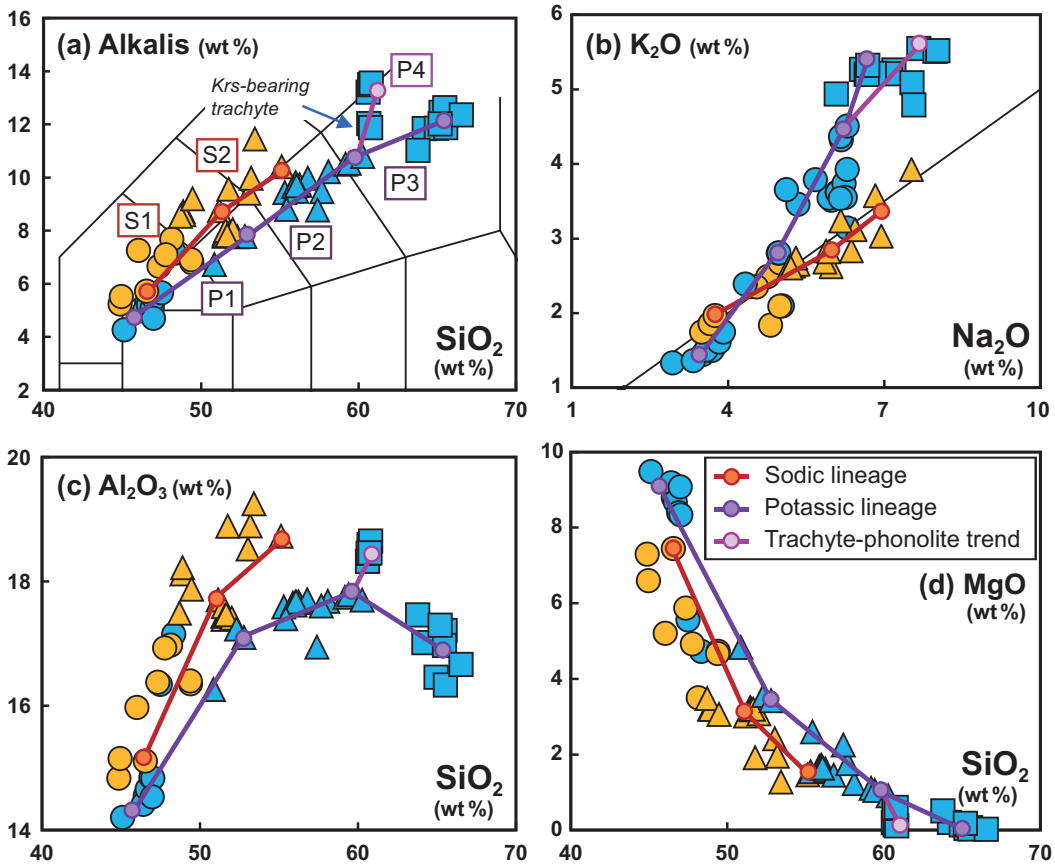

Fig. 9. Magmatic differentiation trends for the potassic (blue symbols) and sodic (yellow symbols) lineages. Calculated model trends (see the key in (d)) are based on assimilation and fractional crystallization mass-balance calculations using the OPTIMASBA Microsoft Excel workbook (Cabero *et al.*, 2012). Modelled sodic trends of S1 and S2, potassic trends P1, P2, and P3, and trachyte–phonolite trend P4 are annotated in (a). Refer to text for details of each trend.

(21), Fe–Ti oxides (10), nepheline (10), and apatite (2). The result agrees with the petrography, which confirms that kaersutite is the dominant fractionating phase in the intermediate sodic lineage.

On the other hand, the petrography suggests that fractionation of the potassic lineage is dominated by olivine and clinopyroxene in the early stage and plagioclase in the later stage. The mass balance model suggests that the evolution from a parental hawaiite (J14120503-2, MgO = 8·3 wt %) to a mugearite (J14120106-1, MgO = 3·4 wt %) is best explained by 48 wt % fractionation with the mineral assemblage (wt %) of olivine (15), clinopyroxene (48), plagioclase (27), Fe–Ti oxides (9), and apatite (1), combined with crustal assimilation to varying degrees from 9 to 17 wt %, depending on the contaminant used for the model (trend P1, Fig. 9). The extensive fractionation of clinopyroxene is consistent with its high abundance in hawaiite and mugearite. Although MgO-rich (>5 wt %) lava samples lack Fe–Ti oxide microphenocrysts, later involvement of significant oxide fractionation is supported by abundant oxide phenocrysts in the mugearite. The crustal contamination effectively lowers the Na, K, and Al contents in the magma, resulting in the potassic nature of these rocks (i.e. mugearite). Details on the effect of crustal assimilation are discussed below.

Fractional crystallization from mugearite (J14120106-1, SiO_2=52·8 wt %) to trachyte (K16012708-1, SiO_2= 59·2 wt %) can be modelled by ~40 wt % fractionation of olivine (14), clinopyroxene (14), plagioclase (55), Fe–Ti oxides (13), and apatite (3), without assimilation of crustal material (trend P2, Fig. 9). The abundant (>50%) plagioclase and increased amounts of Fe–Ti oxide phenocrysts in the mugearite and benmoreite samples are consistent with this model.

The differentiation from trachyte sample K16012707-1 (SiO_2=60 wt %) to a highly-evolved trachytic sample (K16012422-1, SiO_2=64 wt %) is also calculated (Table 5; Fig. 9). Aegirine was included in the model following Kyle (1986). The result suggests that the differentiation can be attributed to 57 wt % fractionation of sanidine (52), plagioclase (30), hedenbergite and aegirine (6), olivine (6), magnetite (5), and apatite (1) (trend P3, Fig. 9). Because most feldspar in the trachyte is sanidine, which is absent in the less evolved lava suites, the gradual change of fractionating feldspar from sodic

Table 5: Calculated fractionated mineral assemblages of The Pleiades lineages using least-squares fractional crystallization and assimilation modeling

	Sodic lineage			Potassic lineage			
Stage	basanite – Phonotephrite	phonotephrite – Tephriphonolite	tephriphonolite – phonolite	hawaiite – mugearite	mugearite – trachyte	trachyte – trachyte	trachyte – phonolite
Parent	K16012708-4	K16012713-2	K16012713-1	J14120503-2	J14120106-1	K16012707-1	K16012707-1
Daughter	K16012713-2	K16012713-1	K16012415	J14120106-1	K16012708-1	K16012422-1	M16012701
Ol (%)	8·1	–	6·8	19·3	14·2	5·9	6·9
Pl	14·8	20·6	–	33·7	55·1	29·6	–
Sa/Ano†	–	–	0/60·6	–	–	52·5/0	44·6/36·2
Aug/Aeg*	33·2	21	3	59·7	14·5	1/4·8	3·2
Krs	35·8	36·2	17·7	–	–	–	8·3
Mt/Ilm‡	6·2/1	10·4	3·1	11/0·4	5/8·2	5·3	<0·1/0·8
Ap†	0·9	2·3	1·6	0·8	3·1	0·9	–
Ne	–	9·6	7·1	–	–	–	–
Contaminant	–	–	–	−24·9	–	–	–
F.C. (%)	45·5	27·7	64·3	38·6	39·8	64·9	89·7
SSE	0·002	0·102	0·048	0·101	0·035	0·048	0·000
R^2	1·000	1·000	1·000	1·000	1·000	1·000	1·000

F.C., amount of crystallization from the parent melt; SEE, sum of squared errors; Ano, anorthoclase; Aug, augite; Aeg, aegirine–augite; Ap, apatite. Details on the calculation are presented in Supplementary Data C.
*Aegirine–augite and apatite compositions adopted from previous mineral data in Kyle (1986).
†Anorthoclase composition adopted from Kelly *et al.* (2008) where anorthoclase phenocryst compositions in Erebus volcanic bombs are reported.
‡Numbers without slash (/) denotes 0% involvement of aegirine-augite or ilmenite.

plagioclase into sanidine during the formation of the trachytic melt is expected. The strong fractionation of feldspar causes the decrease in Al_2O_3, and the negative anomalies of Ba, Sr, and Eu in the primitive mantle-normalized trace element patterns of the highly-evolved trachyte samples (Fig. 6e).

In summary, the mass balance models show kaersutite and clinopyroxene are strongly fractionated in the sodic lineage with relatively minor plagioclase fractionation, whereas strong plagioclase and prolonged olivine fractionation without any kaersutite drove the evolution of the potassic lineage. This difference caused the sharp increase of the K_2O/Na_2O ratio in the potassic lineage due to the low K_2O/Na_2O ratio of plagioclase (Fig. 3b). Additionally, slight elevation of MgO, TiO_2, and FeO_t in the intermediate potassic lavas compared to the sodic ones can be ascribed to their incompatible nature in plagioclase. These are consistent with the variation of trace element abundances. The Sr contents in the potassic lineage sharply decrease during magma differentiation, whereas the sodic lineage retains high Sr concentrations (>800 ppm) (Fig. 5d). The fast depletion of Sc, V, and Co in the sodic lineage can be accounted for by strong fractionation of kaersutite and clinopyroxene, and suppression of plagioclase fractionation, because these transitional metals are compatible in kaersutite and clinopyroxene (Villemant *et al.*, 1981; Tiepolo *et al.*, 2007).

Experimental studies have shown that high H_2O concentration is one of the major factors controlling kaersutite fractionation, and suppressing plagioclase crystallization in mafic to intermediate suites (e.g. Nekvasil *et al.*, 2004; Caricchi *et al.*, 2006; Iacovino *et al.*, 2016). Also, calculations based on the mineral modal proportions in the Chaîne des Puys (French Massif Central) trachyte suggests that at least 1·5 wt % of water is required for parental alkalic basaltic magma to fractionate kaersutite (Martel *et al.*, 2013). At Mt. Erebus, about 1 wt % difference in H_2O contents is enough to result in contrasting fractionation trends with and without kaersutite (Oppenheimer *et al.*, 2011; Rasmussen *et al.*, 2017).

Phonolite lavas

Three phonolite samples (M16012701, K16012425, and K16012415) have elevated Al_2O_3 contents (≥18 wt %) and are distinct from the decreasing Al_2O_3 trend from benmoreite to trachyte compositions (Fig. 4b). It has been suggested that phonolite can be formed by fractional crystallization of strongly alkalic melts (Kyle *et al.*, 1992; Panter *et al.*, 1997; Thompson *et al.*, 2001; Bryan *et al.*, 2002; Martin *et al.*, 2010; Jung *et al.*, 2013) or by fractionation from trachyte (White *et al.*, 2012; AckermAn *et al.*, 2015). Because of the similar petrology of the sodic lineage and the basanite–phonolite DVDP trend in Ross Island, it would seem that the phonolite is derived from the sodic lineage. However, a compositional gap between tephriphonolite samples, elevated K_2O contents, and isotopic compositions similar to the evolved potassic samples, imply that the phonolite lavas are derived from the potassic lineage.

According to our mass-balance calculation, the phonolite composition can be produced by fractional crystallization from both tephriphonolite and trachyte. If the starting composition was tephriphonolite (K16012713-1, SiO_2=56 wt %), ~ 64 wt % fractionation of anorthoclase (61), kaersutite (18), clinopyroxene (3),

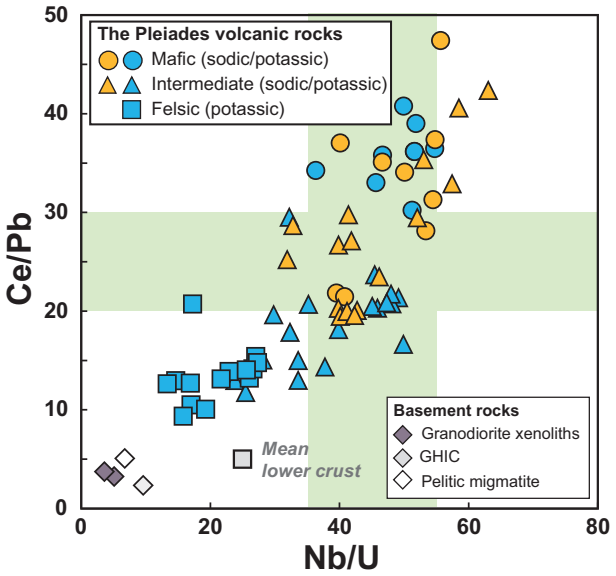

Fig. 10. Ce/Pb vs Nb/U for The Pleiades volcanic rocks and the analysed basement rocks. The light green bars denote the ratios of oceanic basalts (Hofmann, 1986). The grey square denotes the recommended lower continental crust from Rudnick & Gao (2003).

nepheline (7), magnetite (3), and apatite (2) can produce a composition similar to phonolite sample (M16012701). On the other hand, 90 wt % fractionation of anorthoclase (36), sanidine (45), clinopyroxene (3), kaersutite (8), olivine (7), and oxides (1) from the trachytic melt (K16012707-1, SiO_2=60 wt %), can explain the composition of phonolite sample K16012415 (P4 trend in Fig. 9). In both cases, the compositions of plagioclase in the tephriphonolite and benmoreite lavas are too calcic and thus the anorthoclase composition was adopted from Kelly *et al.* (2008).

If the calculation from tephriphonolite to phonolite is correct, the basanite–phonolite trend does not require any crustal contamination. However, the phonolite is isotopically enriched (K16012425, $^{87}Sr/^{86}Sr = 0{\cdot}70397$, $^{143}Nd/^{144}Nd = 0{\cdot}512813$), and addition of a crustal composition as a contaminant in the calculation produces an erroneous result. Also, the calculation is not compatible with sanidine fractionation, which is one of the major phases in the phonolite samples. On the other hand, we found two trachyte samples (M16012710 and M16012714-2) which contain kaersutite pseudomorphs, and these samples show transitional whole-rock compositions between benmoreite and phonolite. The degree of silica-undersaturation in the potassic lineage continuously falls from 5–10 wt % normative nepheline (*ne*) in hawaiites to zero in trachyte, but these two trachyte samples (*ne* = 3·6–4·7 wt %) show increasing trends toward highly silica-undersaturated (*ne* > 10 wt %) phonolite samples. The compositions of these 'transitional' samples match the trachyte–phonolite fractionation modeling trend (Fig. 9). Thus, the phonolite lavas are derivatives of the potassic lineage, aided by late fractionation of kaersutite. Ackerman *et al.* (2015) and White *et al.* (2012) also suggested large amounts, 70–80% and >90% respectively, of amphibole-included fractionating mineral assemblages from trachyte to phonolite, which is broadly similar to our values.

CRUSTAL ASSIMILATION

The fractionation mass-balance model and isotopic data show that the potassic basaltic magmas need crustal assimilation to produce intermediate magmas. Considering that the main fractionating phases lack Na and K, even in the case of plagioclase ($An_{80–60}$, Na_2O+K_2O <5 wt %), the addition of crustal material in the potassic lineage is needed to balance the relatively high alkali contents resulting from differentiation. Conversely, without crustal assimilation, the potassic lineage would follow a trend similar to the sodic lineage, which is the case in other volcanic systems such as Mt. Erebus (Kyle *et al.*, 1992) and Tenerife (Ablay *et al.*, 1998). Wilson *et al.* (1995) suggested that the assimilation process can help exaggerate the compositional variations in basaltic to intermediate magmas, and Schneider *et al.* (2016) also stressed that the assimilation could significantly elevate the degree of silica-saturation in alkalic magmas.

The trace element ratios and Sr–Nd–Pb isotope data from The Pleiades support the addition of crustal materials to the potassic magmas. The Sr concentrations in the potassic lavas decrease below 800 ppm once the SiO_2 content exceeds 50 wt %; similar discontinuities can be found in the trends of Ba, Nb, Eu, and other REE (Fig. 5). The Ce/Pb (9·4–29·5) and Nb/U (13·3–49·9) ratios of the evolved potassic lavas also become much lower than those of the mafic lavas (Ce/Pb = 30–41; Nb/U = 36·3–54·8; Fig. 10), converging toward the average ratios in the crustal materials (Ce/Pb = 3–5·1; Nb/U = 4·4–25; Hacker *et al.*, 2015).

The addition of crustal materials into the potassic magmas is shown in the Sr–Nd–Pb isotope data. The radiogenic signature of $^{87}Sr/^{86}Sr$ (>0·70375) and decreased $^{143}Nd/^{144}Nd$ (<0·51282) in the potassic intermediate lavas are significantly different from the most mafic lavas (Fig. 7a and b; $^{87}Sr/^{86}Sr$ <0·70344 and $^{143}Nd/^{144}Nd$ >0·51287). The Pb isotopic ratios of the evolved potassic lavas ($^{206}Pb/^{204}Pb \leq 19{\cdot}5$; $^{208}Pb/^{204}Pb \leq 39{\cdot}4$) are also shifted toward the lower ratios from the basement. The isotopic ratios of trachyte and phonolite overlap with those of the intermediate lavas, implying that little additional assimilation is required for the felsic suites. This trend is consistent with the mass balance calculation above.

To constrain the crustal contaminants and the degree of assimilation, several possible candidates were examined. Although the xenoliths in The Pleiades are of granodiorite, the majority of the $^{143}Nd/^{144}Nd$ ratios of the evolved potassic lavas are below the mixing trend between the mafic lavas and the granodiorite xenoliths (Fig. 7b). The mixing of the GHIC sample is also inconsistent, because its high Sr content (353 ppm) compared

to Rb (55 ppm) produces a concave-up mixing line (Fig. 7a and b). On the other hand, the mixing lines with granulite or migmatite overlap with most of the isotopic ratios of the evolved lavas. There are some samples whose isotopic ratios are close to the upper crust mixing lines (K16012708-4, K16012425), implying contamination with upper crust material to some extent. Nevertheless, given that the estimated equilibration pressure (5–12 kbar) indicates lower to middle-crustal depths (> 20 km), assimilation of granulite or migmatite is more plausible than of typical upper crustal granitoids.

The amount of crustal material required depends on the bulk-rock composition and isotopic ratios of the candidate crustal rock. The mass balance calculation suggests the composition of intermediate lavas are compatible with the assimilation of 10 wt % migmatite or 9–14 wt % of granulite. The mafic granulite (12B22, SiO_2=49 wt %; Talarico *et al.*, 1995) can be ruled out because an unrealistic amount (~ 24 wt %) of assimilation is required. The predicted amount of crustal materials from the isotope data (5–10%) is slightly lower than that from the mass-balance calculation using major element data (9·6–13·8 wt %). The estimation using the retrogressed felsic granulite (13B29) show the best consistency between the mass balance calculation based on major elements (9·6 wt %) and isotopic ratios (~10 wt %). The migmatite in the Wilson Terrane can also explain the isotopic ratios and major element variations, but the depth at which the migmatite is stable (<6 kbar) is much shallower (Palmeri, 1997) than the lower crust; and thus the 'deep-sited migmatite' would be granulitic after all. Accordingly, roughly 10 wt % assimilation of pelitic granulite best explains the radiogenic isotopic compositions of the evolved lavas of The Pleiades.

The lithology of the lower crust beneath The Pleiades is unknown. Although it can include a variety of rock types, its composition is usually considered to be mafic to intermediate (Hacker *et al.*, 2015). The accretion models for the Ross Orogeny (e.g. Flöttmann & Kleinschmidt, 1991; Federico *et al.*, 2006; Rocchi *et al.*, 2011) depict a (south) westward-dipping paleo-subduction zone and accordingly southwestward-dipping or sub-vertical terrane boundaries. Therefore, the assimilated lower crust beneath The Pleiades could be the underlying pelitic to psammitic fragments of the Bowers Terrane. The inconsistency in the required amount of assimilants between the mass-balance calculation using major element data and isotopic ratios, together with the uncertain nature of the lower crust lithology, suggests that another more suitable end-member may exist beneath The Pleiades.

SOURCES OF THE PRIMITIVE MAGMAS

The petrography and geochemistry data have shown that the volcanic suites in The Pleiades can be divided into two lineages. The two magma evolution trends can be ascribed to distinctive fractionation and crustal assimilation processes between the two lineages. However, the systematic differences in petrology between basanite and hawaiite suggest that the difference of the two lineages, especially of the hydrous and anhydrous characteristics of the sodic and potassic lineages, respectively, may have been inherited from their mantle sources. The input of dry lower crust material may have enhanced dehydration of the potassic lineage, but the difference in the crystallizing mineral assemblages between the two lineages precedes the assimilation process in the differentiation trends. The similar temporal and spatial distribution and the pressure–temperature path between two lineages suggest that a selective increase in the partial pressure of H_2O in the sodic magmas during ascent is also unlikely. In this section, we discuss possible mantle sources and partial melting processes beneath The Pleiades based on the compositions of basanite and hawaiite.

The composition of an intraplate primitive magma is a function of its source composition, pressure and degree of partial melting (Wilson *et al.*, 1995; Panter *et al.*, 1997; Beier *et al.*, 2008; Kolb *et al.*, 2012; McGee *et al.*, 2013, 2015; Pilet, 2015; Baasner *et al.*, 2016). In various volcanic systems, several trace element ratios least affected by fractional crystallization have been used to trace source compositions from melt compositions (Hofmann, 2003). For instance, Hofmann *et al.* (1986) suggested constant ratios of Nb/U (~47) and Ce/Pb (~25) in OIB and mid-ocean ridge basalts (MORB). The mafic lavas from both lineages in The Pleiades share similar ranges of Nb/U (36·3–55·7), Ce/Pb (21·5–47·4), and Nd/Pb (9·5–20·5) (Fig. 10). Also, only a minor difference can be found between the primitive mantle normalized trace element patterns of the two lineages (Fig. 6). This compositional similarity between the mafic lavas from each lineage implies that they share a similar source.

The differentiation of The Pleiades volcanic lineages begins at the silica-poor (SiO_2 <45%) basanite and hawaiite. Because the phenocrysts in the most SiO_2 deficient sample (SiO_2=44·9 wt %) of the sodic lineage are mainly clinopyroxene and kaersutite, the parental magma of the sodic lineage should have more MgO and less SiO_2 than the most mafic sodic samples. Partial melting experiments on dry garnet lherzolite suggest that the major and trace element compositions of silica-poor OIB magmas requires either a non-peridotitic source lithology or addition of volatiles, or both (Davis *et al.*, 2011; Davis & Hirschmann, 2013). It has been suggested that subducted eclogite and pyroxenite could reside in the asthenosphere based on the mineral compositions of various volcanic suites (Hauri, 1996; Sobolev *et al.*, 2005; Prytulak & Elliott, 2007; Herzberg, 2011), experiments (Irving, 1974; Ito & Kennedy, 1974; Hirschmann *et al.*, 2003; Kogiso, 2004) and isotopic data (Chase, 1981; Hofmann & White, 1982; Kokfelt, 2006). Recent studies of mantle xenoliths have suggested that eclogite in the lithospheric mantle is one of the source components of the Cenozoic

magmatism around Victoria Land (Di Vincenzo *et al.*, 1997; Melchiorre *et al.*, 2011; Martin *et al.*, 2015). Alternatively, the occurrence of amphibole- and/or mica-bearing metasomatized mantle rocks has also been recognized (O'Reilly & Griffin, 1988; Haggerty, 1995) and has led to the idea that presence of those minerals in the lithosphere may result in the alkali-enriched nature of the alkalic magmatism (Kushiro *et al.*, 1967; Varne, 1968; Lloyd & Bailey, 1975; Sun & Hanson, 1975; Pilet *et al.*, 2008, 2011; Davis & Hirschmann, 2013).

It is also notable that not all basanite–phonolite alkali-rich trends are hydrous, as in the case of the dry lineages from Mt. Morning and Mt. Erebus (Kyle *et al.*, 1992; Martin *et al.* 2010). For instance, Martin *et al.* (2013) showed that the amphibole-free Riviera Ridge Lineage at Mt. Morning was derived from a nominally anhydrous mantle domain. Conversely, the amphibole-bearing basanite suites from volcanic fields in Madagascar and Germany were inferred to originate from lithospheric mantle containing hydrous minerals (Melluso *et al.*, 2007; Kolb *et al.*, 2012; Jung *et al.*, 2013; Melluso *et al.*, 2018). These observations imply that the mantle source beneath The Pleiades contains hydrous minerals.

The mafic lavas of both lineages of The Pleiades show negative K and positive Nb anomalies in primitive mantle-normalized trace element patterns (Fig. 6). The negative K anomaly suggests the presence of a K-rich residual phase in the melting region. The effect of K-rich mineral fractionation should be negligible because of their mafic nature (MgO >8 wt %) and lack of K-rich phenocrysts in the potassic lavas. Phlogopite and amphibole can be stable at upper mantle conditions (Kushiro *et al.*, 1967; Sato *et al.*, 1997; Sudo & Tatsumi, 1990; Greenough, 1988). The positive Nb and the negative Pb anomalies in the trace element patterns of the mafic lavas are also consistent with the expected melt composition derived from an amphibole-bearing source (Pilet *et al.*, 2011). It has been suggested that absence of Ba fractionation from La in the mafic lavas indicates that amphibole, rather than phlogopite, is the dominant phase in the source (e.g. Jung & Hoernes, 2000; Schubert *et al.*, 2015).

Amphibole- or phlogopite-bearing metasomatized mantle xenoliths has been reported from around Victoria Land (Hornig & Wörner, 1991; Zipfel & Wörner, 1992; Perinelli *et al.*, 2006, 2011; Martin *et al.* 2014, 2015). The stability of amphibole in the upper mantle depends on temperature, pressure, and volatile content. Pargasitic amphibole can be stable at ~3 GPa or less at a maximum temperature of ~1100°C (Dai *et al.*, 2014; Mandler & Grove, 2016). This pressure range broadly matches with the upper level of the low-velocity anomaly beneath the TAM (roughly 60–160 km; Graw *et al.*, 2016) which is interpreted as the partial melting zone (Lawrence *et al.*, 2006; Brenn *et al.*, 2017). The thickness of the lithosphere beneath the TAM is not well constrained, but ten Brink *et al.* (1997) suggested that the elastic thickness of the plate around the TAM is ~ 85 ± 15 km. An *et al.* (2015) suggested 1300–1400°C for the basal (~80 km) temperature of the lithosphere beneath the TAM and that an abnormally high temperature (>1150°C) reaches up to near the Moho boundary. This temperature range for the lithospheric mantle beneath the TAM matches with experiments and Monte Carlo simulated conditions for partial melting of amphibole metasomes (1150–1400°C) (Pilet *et al.*, 2008, 2011). These observations then support the presence of an amphibole- and/or phlogopite-bearing metasomatized lithospheric mantle source beneath The Pleiades.

The elevated $^{206}Pb/^{204}Pb$ (>19·5) and low $^{143}Nd/^{144}Nd$ (<0·51290), together with the negative Pb and positive Nb anomalies and the enrichment of incompatible elements, suggest that the isotopic signature of The Pleiades mantle source can be described as a HIMU component mixed with enriched and depleted sources or, alternatively, as a near-FOZO source (Finn *et al.*, 2005; Sims *et al.*, 2008; Aviado *et al.*, 2015; Fig. 7d). The Pleiades isotopic data overlap with data for Cenozoic volcanic rocks around the Ross Sea, which extend from the HIMU-like Zealandia basalts to the less radiogenic Ross seafloor basalts (Panter *et al.*, 2006, 2018; Timm *et al.*, 2010; Scott *et al.*, 2013; van der Meer *et al.*, 2017). This isotopic signature with a HIMU-affinity is widespread throughout the WARS, Zealandia, and eastern part of the Indo-Australian plate, referred to the as a diffuse alkalic magma province (DAMP; Finn *et al.*, 2005). Because the underlying continental blocks of the DAMP were contiguous before 100 Ma as a part of the margin of Gondwana, their unique compositional variations have been considered to be, at least partly, derived from the common metasomatism of the lithospheric mantle (Coombs *et al.*, 1986; Panter *et al.*, 2000, 2006; Finn *et al.*, 2005; Hoernle *et al.*, 2006; McCoy-West *et al.*, 2010; Timm *et al.*, 2010; Martin *et al.*, 2013; Aviado *et al.*, 2015; Scott *et al.*, 2016; van der Meer *et al.*, 2017).

The details of the causes of this metasomatism and the source of the isotopic signatures are still controversial. Various hypotheses include a fossil mantle plume (Lanyon *et al.*, 1993; Weaver *et al.*, 1994; Rocholl *et al.*, 1995; Hart *et al.*, 1997), subduction-related fluids and melts (Panter *et al.*, 2006; Sprung *et al.*, 2007), mantle upwelling due to the detachment of a subducted slab (Finn *et al.*, 2005) and foundering of the lithospheric mantle (Timm *et al.*, 2010; Shen *et al.*, 2018). Because carbonate can have a high [U+Th]/Pb ratio and high Nb concentrations, recycled carbonate and CO_2-rich melt/carbonatite metasomatized mantle have recently been suggested to be potential intraplate HIMU-like source (Pfänder *et al.*, 2012; Castillo, 2015; McCoy-West *et al.*, 2016). Considering that a carbonatite metasomatic signature in the lithospheric mantle has also been found in the WARS (Martin *et al.*, 2013) and Zealandia (Scott *et al.*, 2014; McCoy-West *et al.*, 2015) and that The

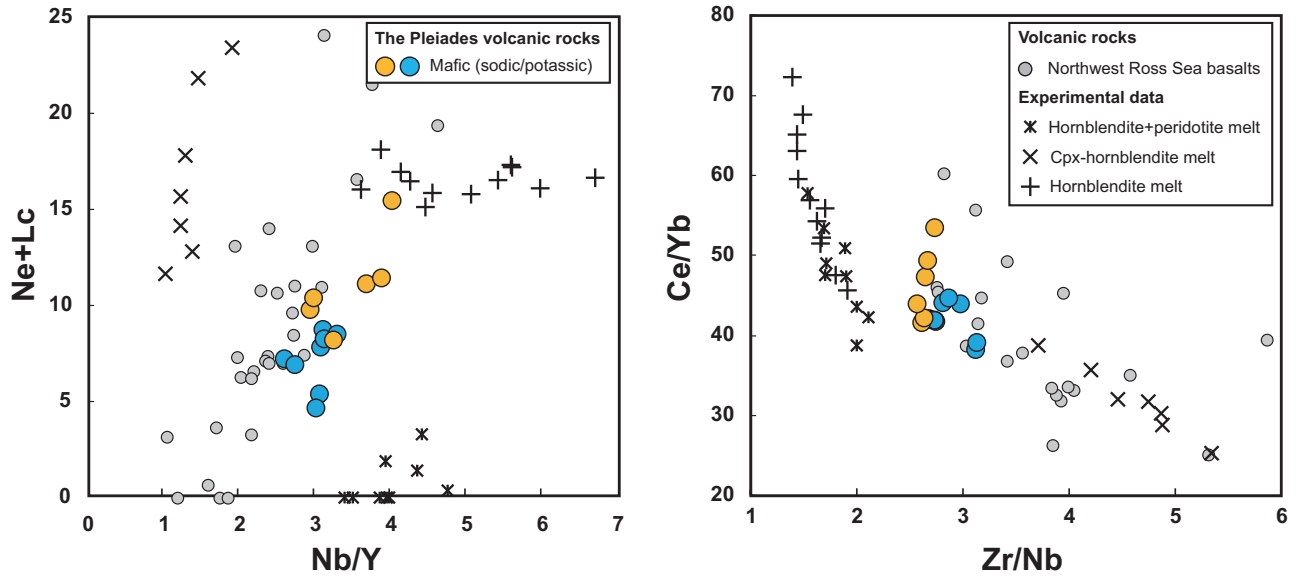

Fig. 11. (a) CIPW normative nepheline+leucite vs Nb/Y and (b) Ce/Yb vs Zr/Nb for The Pleiades volcanic rocks. The basalt compositions from the northwest Ross Sea (Panter *et al.*, 2018) and the melting experiments (Pilet *et al.*, 2008) are also potted. The normative nepheline and leucite contents of The Pleiades volcanic rocks and comparative data were calculated based on the assumption that $Fe^{3+}/Fe_{tot.}$ is 0·2.

Pleiades also show the positive Nb anomaly and the HIMU-like Pb isotopic ratios, The Pleiades magmas may have similar source characteristics and partial melting processes to the DAMP.

PARTIAL MELTING OF THE SOURCE

The formation of and partial melting processes in metasomatized lithospheric mantle have been proposed by a number of authors (e.g. Pilet *et al.*, 2008; Rooney *et al.*, 2014; Pilet, 2015). These authors suggested that previous or contemporary melt percolation and differentiation in the lithospheric mantle forms pyroxene- to amphibole/phlogopite-rich metasomatic veins. Partial melting of these metasomes, with and without interaction with the surrounding peridotite, can produce variably SiO_2-poor alkalic magmas. Also, Pilet *et al.* (2008) showed that the variable degrees of interaction between silica-deficient melts and their surrounding peridotite can explain the compositional variations among nephelinite to alkali–basalt melts.

If the petrogenesis of the parental basaltic magmas at The Pleiades follows this scenario of partial melting of metasomatized lithospheric mantle, the potassic lineage might have resulted from more interaction with the surrounding dry peridotite than the sodic lineage. The lower contents of Al_2O_3, TiO_2, K_2O, and Rb and higher ratios of Zr/Nb (>2·6) in the mafic potassic magmas compared to the sodic ones (Figs 4, 5 and 11b) are consistent with a higher degree of assimilation of the surrounding peridotite (Pilet *et al.*, 2008). Additionally, Panter *et al.* (2018) recently suggested that the systematic variation of the Nb/Y ratio and decrease of the normative nepheline and leucite in the basaltic lavas from the Adare Trough and the Hallett Volcanic Province can be attributed to differences in the degree of involvement of the amphibole-rich metasomes during partial melting in the lithospheric mantle. Indeed, the mafic lavas of the sodic lineage have more normative nepheline and leucite and higher Nb/Y ratios than those of the potassic lineage (Fig. 11a). Considering that the potassic lavas comprise most of The Pleiades lavas, we suggest the more extensive melting of the metasomatized lithosphere has reacted with the surrounding peridotite and produced the potassic magmas, whereas the sodic lineage has been derived from smaller degrees of partial melting of the metasomes.

Heat flux provided by lateral mantle flow, possibly due to mantle upwelling associated with the WARS or lithospheric foundering beneath the TAM, was suggested to trigger the partial melting of metasomes beneath Victoria Land (Nardini *et al.*, 2009; Panter *et al.*, 2018; Shen *et al.*, 2018). The elevated temperature under the lithosphere has produced minor volcanic cones around NVL, which are mostly basanite in composition (Kyle, 1990*b*). Transtensional re-activation of preexisting faults may have enhanced the local thermal anomaly beneath NVL, and produced more voluminous, less silica-undersaturated magmas (Vignaroli *et al.*, 2015). The Pleiades may represent both cases, the former corresponds to the sodic lineage and the latter to the potassic lineage. Similar trends are also observed in other major volcanic fields around NVL. The Melbourne Volcanic Field is mainly composed of hawaiite–trachyte

lavas with peripherally occurring minor amphibole-bearing basanite and tephrite (Kyle, 1990*b*; Giordano *et al.*, 2012). Two lineages similar to The Pleiades have also been reported from Mt. Overlord (Kyle, 1990*b*). Our partial melting model for The Pleiades thus emphasizes the significance of mantle source control on the primitive magma compositions of the NVL volcanoes, or possibly of the intra-continental alkalic magmatism in general.

CONCLUSIONS

The petrological, geochemical and Sr–Nd–Pb isotope dataset from this study provides new insights for the sodic and potassic differentiation lineages at The Pleiades volcanic complex of NVL. The two lineages overlap spatially and temporally. The petrography, geochemistry and the mass-balance calculations show that the potassic lineage can be modelled by the fractionation of anhydrous mineral phases: olivine, clinopyroxene, plagioclase, Fe–Ti oxides with minor apatite. The Sr–Nd–Pb isotopic ratios suggest that the intermediate potassic magma assimilated lower crustal granulite and migmatite. The phonolite and trachyte lavas are the final products of the strong fractional crystallization of the potassic lineage. The crystallizing mineral assemblage of mainly plagioclase and olivine in the potassic lineage points to the anhydrous nature of this lineage. On the other hand, the sodic magma is hydrous, supported by the constant fractionation of kaersutite and the absence of olivine in the intermediate lavas. The pressure and temperature estimations using pyroxene thermobarometry suggest that the mafic to intermediate magmas of both lineages shared similar mama ascent paths, and mostly resided in the lower crust.

The HIMU-like signatures and the positive Nb and negative K anomalies in the mafic lavas argue for an amphibole-rich, metasomatized lithospheric mantle source beneath The Pleiades, which is consistent with the young HIMU-like alkalic volcanism in Zealandia and Antarctica. The compositions of the mafic lavas from the sodic lineage have more affinity towards previously reported hornblendite melt compositions than the potassic lavas. This compositional difference implies that the melts derived from the melting of the metasomes in NVL lithosphere experienced a higher degree of interaction with the surrounding dry peridotite compared to the relatively minor sodic melts. The stronger involvements of the dry peridotite in partial melting also led to the drier nature of the potassic magmas compared to the sodic ones.

This study shows that diverse magma differentiation lineages can be produced even if the lineages are spatially (kilometre-scale) and temporally ($<$1 Ma) indistinguishable within a single intracontinental volcanic complex. The initial difference in the water content of the source which resulted in the two lineages can be enhanced by assimilation of crustal materials. Our data suggest that the HIMU-like magmas in The Pleiades have been sourced from metasomatized lithospheric mantle beneath NVL.

ACKNOWLEDGEMENTS

We thank the KOPRI and USAP G081 team members for the assistance during field work. We are grateful to Jin Hong Kim, David Parmelee, Anne Foster, and Young-Min Kim for help with sample collection and field safety, and to Seunghee Han, Seung-Ah Ha, and Jongmin Baek, who run the ICP-MS and TIMS facilities in KOPRI. Changkun Park, Jeongjin Moon, and Sun Young Park are thanked for supporting EPMA analyses. Yun Seok Yang is thanked for XRF analyses. Also, Sook Ju Kim is thanked for help with the SHRIMP analyses. We also thank Sangbum Park and Pilmo Kang for help with sample preparation. Taehwan Kim is appreciated by providing the migmatite and GHIC samples.
We acknowledge the constructive input of the official Journal of Petrology referees, Adam Martin, Lucy McGee and Bill Landenberger, and Editor John Gamble.

FUNDING

This research was supported by a research fund from KOPRI (20140409, PM18030). We also acknowledge financial support from the Brain Korea (BK) 21 Project and National Research Foundation (NRF; 2017K1A12013180). PRK acknowledges support from the National Science Foundation, Office of Polar Programs grant ANT1142083.

SUPPLEMENTARY DATA

Supplementary data are available at *Journal of Petrology* online.

REFERENCES

Ablay, G., Carroll, M., Palmer, M., Martí, J. & Sparks, R. (1998). Basanite–phonolite lineages of the Teide–Pico Viejo volcanic complex, Tenerife, Canary Islands. *Journal of Petrology* **39**, 905–936.

Ackerman, L., Ulrych, J., Řanda, Z., Erban, V., Hegner, E., Magna, T., Balogh, K., Frána, J., Lang, M. & Novák, J. K. (2015). Geochemical characteristics and petrogenesis of phonolites and trachytic rocks from the České Středohoří Volcanic Complex, the Ohře Rift, Bohemian Massif. *Lithos* **224-225**, 256–271.

An, M., Wiens, D. A., Zhao, Y., Feng, M., Nyblade, A., Kanao, M., Li, Y., Maggi, A. & Lévêque, J. J. (2015). Temperature, lithosphere-asthenosphere boundary, and heat flux beneath the Antarctic Plate inferred from seismic velocities. *Journal of Geophysical Research: Solid Earth* **120**, 8720–8742.

Armienti, P. & Baroni, C. (1999). Cenozoic climatic change in Antarctica recorded by volcanic activity and landscape evolution. *Geology* **27**, 617–620.

Armienti, P., Ghezzo, C., Innocenti, F., Manetti, P., Rocchi, S. & Tonarini, S. (1990). Isotope geochemistry and petrology of granitoid suites from Granite Harbour intrusives of the Wilson Terrane, North Victoria Land, Antarctica. *European Journal of Mineralogy* **2**, 103–124.

Armstrong, R. L. (1978). K-Ar dating: Late Cenozoic McMurdo Volcanic Group and dry valley glacial history, Victoria Land, Antarctica. *New Zealand Journal of Geology and Geophysics* **21**, 685–698.

Aviado, K. B., Rilling-Hall, S., Bryce, J. G. & Mukasa, S. B. (2015). Submarine and subaerial lavas in the West Antarctic Rift System: temporal record of shifting magma source components from the lithosphere and asthenosphere. *Geochemistry, Geophysics, Geosystems* **16**, 4344–4361.

Ayuso, R. A., De Vivo, B., Rolandi, G., Seal, R. R. & Paone, A. (1998). Geochemical and isotopic (Nd–Pb–Sr–O) variations bearing on the genesis of volcanic rocks from Vesuvius, Italy. *Journal of Volcanology and Geothermal Research* **82**, 53–78.

Baasner, A., Médard, E., Laporte, D. & Hoffer, G. (2016). Partial melting of garnet lherzolite with water and carbon dioxide at 3 GPa using a new melt extraction technique: implications for intraplate magmatism. *Contributions to Mineralogy and Petrology* **171**, 45.

Baker, I. (1969). Petrology of the volcanic rocks of Saint Helena island, South Atlantic. *Geological Society of America Bulletin* **80**, 1283–1310.

Bannister, S., Yu, J., Leitner, B. & Kennett, B. (2003). Variations in crustal structure across the transition from West to East Antarctica, Southern Victoria Land. *Geophysical Journal International* **155**, 870–880.

Behrendt, J. C. (1999). Crustal and lithospheric structure of the West Antarctic Rift System from geophysical investigations—a review. *Global and Planetary Change* **23**, 25–44.

Beier, C., Haase, K. M., Abouchami, W., Krienitz, M.-S. & Hauff, F. (2008). Magma genesis by rifting of oceanic lithosphere above anomalous mantle: Terceira Rift, Azores. *Geochemistry, Geophysics, Geosystems* **9**, Q12013.

Block, A. E., Bell, R. E. & Studinger, M. (2009). Antarctic crustal thickness from satellite gravity: implications for the Transantarctic and Gamburtsev Subglacial Mountains. *Earth and Planetary Science Letters* **288**, 194–203.

Borg, S., Stump, E., Chappell, B. W., McCulloch, M., Wyborn, D., Armstrong, R. & Holloway, J. (1987). Granitoids of northern Victoria Land, Antarctica; implications of chemical and isotopic variations to regional crustal structure and tectonics. *American Journal of Science* **287**, 127–169.

Brenn, G. R., Hansen, S. E. & Park, Y. (2017). Variable thermal loading and flexural uplift along the Transantarctic Mountains, Antarctica. *Geology* **45**, 463–466.

Brenna, M., Price, R., Cronin, S. J., Smith, I. E. M., Sohn, Y. K., Kim, G. B. & Maas, R. (2014). Final magma storage depth modulation of explosivity and trachyte–phonolite genesis at an intraplate volcano: a case study from Ulleung Island, South Korea. *Journal of Petrology* **55**, 709–747.

Brenna, M., Nakada, S., Miura, D., Toshida, K., Ito, H., Hokanishi, N. & Nakai, S. I. (2015). A trachyte–syenite core within a basaltic nest: filtering of primitive injections by a multi-stage magma plumbing system (Oki-Dōzen, south-west Japan). *Contributions to Mineralogy and Petrology* **170**, 22.

Bryan, S., Marti, J. & Leosson, M. (2002). Petrology and geochemistry of the bandas del Sur formation, Las Cañadas edifice, Tenerife (Canary Islands). *Journal of Petrology* **43**, 1815–1856.

Cabero, M. T., Mecoleta, S. & López-Moro, F. J. (2012). OPTIMASBA: a Microsoft Excel workbook to optimise the mass-balance modelling applied to magmatic differentiation processes and subsolidus overprints. *Computers & Geosciences* **42**, 206–211.

Caricchi, L., Ulmer, P. & Peccerillo, A. (2006). A high-pressure experimental study on the evolution of the silicic magmatism of the Main Ethiopian Rift. *Lithos* **91**, 46–58.

Castillo, P. R. (2015). The recycling of marine carbonates and sources of HIMU and FOZO ocean island basalts. *Lithos* **216**, 254–263.

Chang, J. M., Feeley, T. C. & Deraps, M. R. (2009). Petrogenesis of Basaltic Volcanic Rocks from the Pribilof Islands, Alaska, by melting of metasomatically enriched depleted lithosphere, crystallization differentiation, and magma mixing. *Journal of Petrology* **50**, 2249–2286.

Chaput, J., Aster, R. C., Huerta, A., Sun, X., Lloyd, A., Wiens, D., Nyblade, A., Anandakrishnan, S., Winberry, J. P. & Wilson, T. (2014). The crustal thickness of West Antarctica. *Journal of Geophysical Research: Solid Earth* **119**, 378–395.

Chase, C. G. (1981). Oceanic island Pb: two-stage histories and mantle evolution. *Earth and Planetary Science Letters* **52**, 277–284.

Cheong, W., Cho, M. & Kim, Y. (2013). An efficient method for zircon separation using the gold pan. *The Journal of the Petrological Society of Korea* **22**, 63–70.

Class, C. & Goldstein, S. L. (1997). Plume-lithosphere interactions in the ocean basins: constraints from the source mineralogy. *Earth and Planetary Science Letters* **150**, 245–260.

Coombs, D. & Wilkinson, J. (1969). Lineages and fractionation trends in undersaturated volcanic rocks from the East Otago volcanic province (New Zealand) and related rocks. *Journal of Petrology* **10**, 440–501.

Coombs, D. S., Cas, R. A., Kawachi, Y., Landis, C. A., McDonough, W. F. & Reay, A. (1986). Cenozoic volcanism in North, East, and Central Otago. In: Smith, I. E. M. (ed.) *Late Cenozoic Volcanism in New Zealand*, Volume **23**. Wellington: Royal Society of New Zealand Bulletin, pp. 278–312.

Cooper, R. A., Jago, J. B., Rowell, A. J. & Braddock, P. (1983). Age and correlation of the Cambro-Ordovician Bowers Supergroup, northern Victoria Land. In: Olivier, R. L., James, P. R. & Jago, J. B. (eds) *Antarctic Earth Science*. Canberra: Australian Academy of Science, pp. 128–131.

Correale, A., Paonita, A., Martelli, M., Rizzo, A., Rotolo, S. G., Corsaro, R. A. & Di Renzo, V. (2014). A two-component mantle source feeding Mt. Etna magmatism: insights from the geochemistry of primitive magmas. *Lithos* **184**, 243–258.

Dai, L.-Q., Zhao, Z.-F. & Zheng, Y.-F. (2014). Geochemical insights into the role of metasomatic hornblendite in generating alkali basalts. *Geochemistry, Geophysics, Geosystems* **15**, 3762–3779.

Dallai, L., Ghezzo, C. & Sharp, Z. (2003). Oxygen isotope evidence for crustal assimilation and magma mixing in the Granite Harbour Intrusives, Northern Victoria Land, Antarctica. *Lithos* **67**, 135–151.

Dasgupta, R., Hirschmann, M. M. & Smith, N. D. (2007). Partial melting experiments of peridotite+CO_2 at 3 GPa and genesis of alkalic ocean island basalts. *Journal of Petrology* **48**, 2093–2124.

Davis, F., Hirschmann, M. & Humayun, M. (2011). The composition of the incipient partial melt of garnet peridotite at 3GPa and the origin of OIB. *Earth and Planetary Science Letters* **308**, 380–390.

Davis, F. A. & Hirschmann, M. M. (2013). The effects of K_2O on the compositions of near-solidus melts of garnet peridotite at 3 GPa and the origin of basalts from enriched mantle. *Contributions to Mineralogy and Petrology* **166**, 1029–1046.

Decesari, R. C., Wilson, D., Luyendyk, B. P., Faulkner, M., (2007). Cretaceous and tertiary extension throughout the Ross Sea, Antarctica. In: Cooper, A. K. et al. (eds). *A Keystone in a Changing World – Online Proceedings of the 10th ISAES*, Short Research Paper 098, pp. 6, doi:0.333/of2007–1047. srp098.

Deer, W. A., Howie, R. A. & Zussman, J. (2013). *An Introduction to the Rock-forming Minerals*, 3rd edition. London: The Mineralogical Society.

Del Carlo, P., Di Roberto, A., Di Vincenzo, G., Bertagnini, A., Landi, P., Pompilio, M., Colizza, E. & Giordano, G. (2015). Late Pleistocene-Holocene volcanic activity in northern Victoria Land recorded in Ross Sea (Antarctica) marine sediments. *Bulletin of Volcanology* **77**, 1.

Di Vincenzo, G. & Rocchi, S. (1999). Origin and interaction of mafic and felsic magmas in an evolving late orogenic setting: the Early Paleozoic Terra Nova Intrusive Complex, Antarctica. *Contributions to Mineralogy and Petrology* **137**, 15–35.

Di Vincenzo, G., Palmeri, R., Talarico, F., Andriessen, P. & Ricci, G. (1997). Petrology and geochronology of eclogites from the Lanterman Range, Antarctica. *Journal of Petrology* **38**, 1391–1417.

Elliot, D. H. (2013). The geological and tectonic evolution of the Transantarctic Mountains: a review. *Geological Society, London, Special Publications* **381**, 7–35.

Esser, R. P. & Kyle, P. R. (2002). $^{40}Ar/^{39}Ar$ chronology of the McMurdo Volcanic Group at The Pleiades, northern Victoria Land, Antarctica. In: Gamble J. A., Skinner D. N. B. & Henrys, S. (eds) *Antarctica at the close of a millenium, proceedings of the 8th International Symposium on Antarctic Earth Sciences*, Wellington: Royal Society of New Zealand Bulletin, Volume **35**, pp. 415–418.

Federico, L., Capponi, G. & Crispini, L. (2006). The Ross orogeny of the transantarctic mountains: a northern Victoria Land perspective. *International Journal of Earth Sciences* **95**, 759–770.

Finn, C. A., Müller, R. D. & Panter, K. S. (2005). A Cenozoic diffuse alkaline magmatic province (DAMP) in the southwest Pacific without rift or plume origin. *Geochemistry, Geophysics, Geosystems* **6**, Q02005.

Fitton, J. G. & Godard, M. (2004). Origin and evolution of magmas on the Ontong Java Plateau. *Geological Society, London, Special Publications* **229**, 151–178.

Flöttmann, T. & Kleinschmidt, G. (1991). Opposite thrust systems in northern Victoria Land, Antarctica: imprints of Gondwana's Paleozoic accretion. *Geology* **19**, 45–47.

Foland, K., Landoll, J., Henderson, C. & Chen, J. (1993). Formation of cogenetic quartz and nepheline syenites. *Geochimica et Cosmochimica Acta* **57**, 697–704.

Freundt, A. & Schmincke, H. U. (1995). Petrogenesis of rhyolite--trachyte-basalt composite ignimbrite P1, Gran Canada, Canary Islands. *Journal of Geophysical Research: Solid Earth* **100**, 455–474.

Genske, F. S., Turner, S. P., Beier, C. & Schaefer, B. F. (2012). The Petrology and Geochemistry of Lavas from the Western Azores Islands of Flores and Corvo. *Journal of Petrology* **53**, 1673–1708.

Gerbode, C. & Dasgupta, R. (2010). Carbonate-fluxed melting of MORB-like pyroxenite at 2.9 GPa and genesis of HIMU ocean island basalts. *Journal of Petrology* **51**, 2067–2088.

Giacomoni, P. P., Coltorti, M., Bryce, J. G., Fahnestock, M. F. & Guitreau, M. (2016). Mt. Etna plumbing system revealed by combined textural, compositional, and thermobarometric studies in clinopyroxenes. *Contributions to Mineralogy and Petrology* **171**, 34.

Giordano, G., Lucci, F., Phillips, D., Cozzupoli, D. & Runci, V. (2012). Stratigraphy, geochronology and evolution of the Mt. Melbourne volcanic field (North Victoria Land, Antarctica). *Bulletin of Volcanology* **74**, 1–21.

Grant, T. B., Milke, R., Pandey, S. & Jahnke, H. (2013). The Heldburg Phonolite, Central Germany: reactions between phonolite and xenocrysts from the upper mantle and lower crust. *Lithos* **182-183**, 86–101.

Graw, J. H., Adams, A. N., Hansen, S. E., Wiens, D. A., Hackworth, L. & Park, Y. (2016). Upper mantle shear wave velocity structure beneath northern Victoria Land, Antarctica: volcanism and uplift in the northern Transantarctic Mountains. *Earth and Planetary Science Letters* **449**, 48–60.

Green, D. (1973a). Contrasted melting relations in a pyrolite upper mantle under mid-oceanic ridge, stable crust and island arc environments. *Tectonophysics* **17**, 285–297.

Green, D. (1973b). Conditions of melting of basanite magma from garnet peridotite. *Earth and Planetary Science Letters* **17**, 456–465.

Greenough, J. D. (1988). Minor phases in the Earth's mantle: evidence from trace-and minor-element patterns in primitive alkaline magmas. *Chemical Geology* **69**, 177–192.

Hacker, B. R., Kelemen, P. B. & Behn, M. D. (2015). Continental lower crust. *Annual Review of Earth and Planetary Sciences* **43**, 167–205.

Haggerty, S. E. (1995). Upper mantle mineralogy. *Journal of Geodynamics* **20**, 331–364.

Hammer, J., Cashman, K., Hoblitt, R. & Newman, S. (1999). Degassing and microlite crystallization during pre-climactic events of the 1991 eruption of Mt. Pinatubo, Philippines. *Bulletin of Volcanology* **60**, 355–380.

Hansen, S. E., Graw, J. H., Kenyon, L. M., Nyblade, A. A., Wiens, D. A., Aster, R. C., Huerta, A. D., Anandakrishnan, S. & Wilson, T. (2014). Imaging the Antarctic mantle using adaptively parameterized P-wave tomography: evidence for heterogeneous structure beneath West Antarctica. *Earth and Planetary Science Letters* **408**, 66–78.

Hansen, S. E., Kenyon, L. M., Graw, J. H., Park, Y. & Nyblade, A. A. (2016). Crustal structure beneath the northern Transantarctic Mountains and Wilkes subglacial basin: implications for tectonic origins. *Journal of Geophysical Research: Solid Earth* **121**, 812–825.

Hansen, S. E., Reusch, A. M., Parker, T., Bloomquist, D. K., Carpenter, P., Graw, J. H. & Brenn, G. R. (2015). The Transantarctic Mountains Northern Network (TAMNNET): deployment and performance of a seismic array in Antarctica. *Seismological Research Letters* **86**, 1636–1644.

Hart, S. R., Blusztajn, J., LeMasurier, W. E. & Rex, D. C. (1997). Hobbs Coast Cenozoic volcanism: implications for the West Antarctic rift system. *Chemical Geology* **139**, 223–248.

Hauri, E. H. (1996). Major-element variability in the Hawaiian mantle plume. *Nature* **382**, 415–419.

Hawthorne, F. C., Oberti, R., Harlow, G. E., Maresch, W. V., Martin, R. F., Schumacher, J. C. & Welch, M. D. (2012). Nomenclature of the amphibole supergroup. *American Mineralogist* **97**, 2031–2048.

Henjes-Kunst, F. & Schussler, U. (2003). Metasedimentary units of the Cambro-Ordovician Ross Orogen in northern Victoria Land and Oates Land: implications for their provenance and geotectonic setting from geochemical and Nd-Sr isotope data. *Terra Antartica* **10**, 105–128.

Herzberg, C. (2011). Identification of source lithology in the Hawaiian and Canary Islands: implications for origins. *Journal of Petrology* **52**, 113–146.

Hirose, K. (1997). Partial melt compositions of carbonated peridotite at 3 GPa and role of CO_2 in alkali-basalt magma generation. *Geophysical Research Letters* **24**, 2837–2840.

Hirschmann, M. M., Kogiso, T., Baker, M. B. & Stolper, E. M. (2003). Alkalic magmas generated by partial melting of garnet pyroxenite. *Geology* **31**, 481–484.

Hoblitt, R. P. & Harmon, R. S. (1993). Bimodal density distribution of cryptodome dacite from the 1980 eruption of Mount St. Helens, Washington. *Bulletin of Volcanology* **55**, 421–437.

Hoernle, K., White, J. D. L., van den Bogaard, P., Hauff, F., Coombs, D. S., Werner, R., Timm, C., Garbe-Schönberg, D., Reay, A. & Cooper, A. F. (2006). Cenozoic intraplate volcanism on New Zealand: upwelling induced by lithospheric removal. *Earth and Planetary Science Letters* **248**, 350–367.

Hofmann, A. (2003). Sampling mantle heterogeneity through oceanic basalts: isotopes and trace elements. *Treatise on Geochemistry* **2**, 568.

Hofmann, A., Jochum, K., Seufert, M. & White, W. (1986). Nb and Pb in oceanic basalts: new constraints on mantle evolution. *Earth and Planetary Science Letters* **79**, 33–45.

Hofmann, A. W. & White, W. M. (1982). Mantle plumes from ancient oceanic crust. *Earth and Planetary Science Letters* **57**, 421–436.

Hole, M. & LeMasurier, W. (1994). Tectonic controls on the geochemical composition of Cenozoic, mafic alkaline volcanic rocks from West Antarctica. *Contributions to Mineralogy and Petrology* **117**, 187–202.

Hornig, I. & Wörner, G. (1991). Zirconolite-bearing ultra-potassic veins in a mantle-xenolith from Mt. Melbourne Volcanic Field, Victoria Land, Antarctica. *Contributions to Mineralogy and Petrology* **106**, 355–366.

Iacovino, K., Oppenheimer, C., Scaillet, B. & Kyle, P. (2016). Storage and evolution of mafic and intermediate alkaline magmas beneath Ross Island, Antarctica. *Journal of Petrology* **57**, 93–118.

Irving, A. (1974). Geochemical and high pressure experimental studies of garnet pyroxenite and pyroxene granulite xenoliths from the Delegate basaltic pipes, Australia. *Journal of Petrology* **15**, 1–40.

Ito, K. & Kennedy, G. C. (1974). The composition of liquids formed by partial melting of eclogites at high temperatures and pressures. *The Journal of Geology* **82**, 383–392.

Jakobsson, S. P., Pedersen, A., Rønsbo, J. & Larsen, L. M. (1973). Petrology of mugearite-hawaiite: early extrusives in the 1973 Heimaey eruption, Iceland. *Lithos* **6**, 203–214.

Jochum, K. P., Nohl, U., Herwig, K., Lammel, E., Stoll, B. & Hofmann, A. W. (2005). GeoReM: a new geochemical database for reference materials and isotopic standards. *Geostandards and Geoanalytical Research* **29**, 333–338.

Jung, S. & Hoernes, S. (2000). The major-and trace-element and isotope (Sr, Nd, O) geochemistry of Cenozoic alkaline rift-type volcanic rocks from the Rhön area (central Germany): petrology, mantle source characteristics and implications for asthenosphere–lithosphere interactions. *Journal of Volcanology and Geothermal Research* **99**, 27–53.

Jung, S., Mezger, K., Hauff, F., Pack, A. & Hoernes, S. (2013). Petrogenesis of rift-related tephrites, phonolites and trachytes (Central European Volcanic Province, Rhön, FRG): constraints from Sr, Nd, Pb and O isotopes. *Chemical Geology* **354**, 203–215.

Jung, S., Vieten, K., Romer, R. L., Mezger, K., Hoernes, S. & Satir, M. (2012). Petrogenesis of tertiary alkaline magmas in the Siebengebirge, Germany. *Journal of Petrology* **53**, 2381–2409.

Kelly, P. J., Kyle, P. R., Dunbar, N. W. & Sims, K. W. W. (2008). Geochemistry and mineralogy of the phonolite lava lake, Erebus volcano, Antarctica: 1972–2004 and comparison with older lavas. *Journal of Volcanology and Geothermal Research* **177**, 589–605.

Kienle, J., Kyle, P. R., Self, S., Motyka, R. J. & Lorenz, V. (1980). Ukinrek Maars, Alaska, I. April 1977 eruption sequence, petrology and tectonic setting. *Journal of Volcanology and Geothermal Research* **7**, 11–37.

Kogiso, T. (2004). High-pressure partial melting of mafic lithologies in the mantle. *Journal of Petrology* **45**, 2407–2422.

Kokfelt, T. F. (2006). Combined trace element and Pb-Nd-Sr-O isotope evidence for recycled oceanic crust (upper and lower) in the Iceland Mantle Plume. *Journal of Petrology* **47**, 1705–1749.

Kolb, M., Paulick, H., Kirchenbaur, M. & Münker, C. (2012). Petrogenesis of Mafic to Felsic Lavas from the Oligocene Siebengebirge Volcanic Field (Germany): implications for the origin of intracontinental volcanism in Central Europe. *Journal of Petrology* **53**, 2349–2379.

Kuritani, T., Kimura, J.-I., Miyamoto, T., Wei, H., Shimano, T., Maeno, F., Jin, X. & Taniguchi, H. (2009). Intraplate magmatism related to deceleration of upwelling asthenospheric mantle: implications from the Changbaishan shield basalts, northeast China. *Lithos* **112**, 247–258.

Kushiro, I., Syono, Y. & Akimoto, S-I. (1967). Stability of phlogopite at high pressures and possible presence of phlogopite in the earth's upper mantle. *Earth and Planetary Science Letters* **3**, 197–203.

Kyle, P. R. (1981). Mineralogy and geochemistry of a basanite to phonolite sequence at Hut Point Peninsula, Antarctica, based on core from Dry Valley Drilling Project Drillholes 1, 2 and 3. *Journal of Petrology* **22**, 451–500.

Kyle, P. R. (1982). Volcanic geology of the Pleiades, Northern Victoria Land, Antarctica. In: Craddock, C. (ed.) *Antarctic Geoscience*. Madison: University of Wisconsin Press, pp. 747–754.

Kyle, P. R. (1986). Mineral chemistry of late Cenozoic McMurdo Volcanic Group rocks from the Pleiades, Northern Victoria Land. *Geological Investigations in Northern Victoria Land* **305**, 337.

Kyle, P. R. (1990a). McMurdo Volcanic Group Western Ross Embayment: introduction. In: LeMasurier, W. & Thompson, J. (eds) *Volcanism of the Antarctic Plate and Southern Oceans. Antarctic Research Series*, Volume **48**. Washington D.C.: American Geophysical Union, pp. 18–25.

Kyle, P. R. (1990b). Melbourne volcanic province: summary. In: LeMasurier, W. & Thompson, J. (eds) *Volcanism of the Antarctic Plate and Southern Oceans. Antarctic Research Series*, Volume **48**. Washington D.C.: American Geophysical Union, pp. 48–52.

Kyle, P. R. & Rankin, P. C. (1976). Rare earth element geochemistry of Late Cenozoic alkaline lavas of the McMurdo Volcanic Group, Antarctica. *Geochimica et Cosmochimica Acta* **40**, 1497–1507.

Kyle, P. R., Moore, J. & Thirlwall, M. (1992). Petrologic evolution of anorthoclase phonolite lavas at Mount Erebus, Ross Island, Antarctica. *Journal of Petrology* **33**, 849–875.

Lanyon, R., Varne, R. & Crawford, A. J. (1993). Tasmanian Tertiary basalts, the Balleny plume, and opening of the Tasman Sea (southwest Pacific Ocean). *Geology* **21**, 555–558.

Laporte, D., Lambart, S., Schiano, P. & Ottolini, L. (2014). Experimental derivation of nepheline syenite and phonolite liquids by partial melting of upper mantle peridotites. *Earth and Planetary Science Letters* **404**, 319–331.

Lawrence, J. F., Wiens, D. A., Nyblade, A. A., Anandakrishnan, S., Shore, P. J. & Voigt, D. (2006). Crust and upper mantle structure of the Transantarctic Mountains and surrounding regions from receiver functions, surface waves, and gravity: implications for uplift models. *Geochemistry, Geophysics, Geosystems* **7**, Q10011.

Le Bas, M. J., Le Maitre, R. W., Streckeisen, A. & Zanettin, B. (1986). A chemical classification of volcanic rocks based on the total alkali-silica diagram. *Journal of Petrology* **27**, 745–750.

Le Roex, A. P., Cliff, R. & Adair, B. (1990). Tristan da Cunha, South Atlantic: geochemistry and petrogenesis of a basanite-phonolite lava series. *Journal of Petrology* **31**, 779–812.

Lee, M. J., Lee, J. I., Kim, T. H., Lee, J. & Nagao, K. (2015). Age, geochemistry and Sr-Nd-Pb isotopic compositions of alkali volcanic rocks from Mt. Melbourne and the western Ross Sea, Antarctica. *Geosciences Journal* **19**, 681–695.

Lindsley, D. H. (1983). Pyroxene thermometry. *American Mineralogist* **68**, 477–493.

Lloyd, F. & Bailey, D. (1975). Light element metasomatism of the continental mantle: the evidence and the consequences. *Physics and Chemistry of the Earth* **9**, 389–416.

Lucassen, F., Pudlo, D., Franz, G., Romer, R. L. & Dulski, P. (2013). Cenozoic intra-plate magmatism in the Darfur volcanic province: mantle source, phonolite-trachyte genesis and relation to other volcanic provinces in NE Africa. *International Journal of Earth Sciences* **1**, 23.

Mandler, B. E. & Grove, T. L. (2016). Controls on the stability and composition of amphibole in the Earth's mantle. *Contributions to Mineralogy and Petrology* **171**, 68.

Martel, C., Champallier, R., Prouteau, G., Pichavant, M., Arbaret, L., Balcone-Boissard, H., Boudon, G., Boivin, P., Bourdier, J. L. & Scaillet, B. (2013). Trachyte Phase Relations and Implication for Magma Storage Conditions in the Chaîne des Puys (French Massif Central). *Journal of Petrology* **54**, 1071–1107.

Martin, A. P., Cooper, A. F. & Dunlap, W. J. (2010). Geochronology of Mount Morning, Antarctica: two-phase evolution of a long-lived trachyte-basanite-phonolite eruptive center. *Bulletin of Volcanology* **72**, 357–371.

Martin, A. P., Cooper, A. F. & Price, R. C. (2013). Petrogenesis of Cenozoic, alkalic volcanic lineages at Mount Morning, West Antarctica and their entrained lithospheric mantle xenoliths: lithospheric versus asthenospheric mantle sources. *Geochimica et Cosmochimica Acta* **122**, 127–152.

Martin, A. P., Price, R. C. & Cooper, A. F. (2014). Constraints on the composition, source and petrogenesis of plagioclase-bearing mantle peridotite. *Earth-Science Reviews* **138**, 89–101.

Martin, A. P., Price, R. C., Cooper, A. F. & McCammon, C. A. (2015). Petrogenesis of the rifted southern Victoria Land lithospheric mantle, Antarctica, inferred from petrography, geochemistry, thermobarometry and oxybarometry of peridotite and pyroxenite xenoliths from the Mount Morning eruptive centre. *Journal of Petrology* **56**, 193–226.

Masotta, M., Mollo, S., Freda, C., Gaeta, M. & Moore, G. (2013). Clinopyroxene-liquid thermometers and barometers specific to alkaline differentiated magmas. *Contributions to Mineralogy and Petrology* **166**, 1545.

McCoy-West, A. J., Baker, J. A., Faure, K. & Wysoczanski, R. (2010). Petrogenesis and origins of mid-cretaceous continental intraplate volcanism in Marlborough, New Zealand: implications for the long-lived HIMU magmatic Mega-province of the SW Pacific. *Journal of Petrology* **51**, 2003–2045.

McCoy-West, A. J., Bennett, V. C. & Amelin, Y. (2016). Rapid Cenozoic ingrowth of isotopic signatures simulating "HIMU" in ancient lithospheric mantle: distinguishing source from process. *Geochimica et Cosmochimica Acta* **187**, 79–101.

McCoy-West, A. J., Bennett, V. C., O'Neill, H. S. C., Hermann, J. & Puchtel, I. S. (2015). The interplay between melting, refertilization and carbonatite metasomatism in off-cratonic lithospheric mantle under Zealandia: an integrated major, trace and platinum group element study. *Journal of Petrology* **56**, 563–604.

McDonough, W. F. & Sun, S.-S. (1995). The composition of the Earth. *Chemical Geology* **120**, 223–253.

McGee, L. E., Millet, M. A., Beier, C., Smith, I. E. M. & Lindsay, J. M. (2015). Mantle heterogeneity controls on small-volume basaltic volcanism. *Geology* **43**, 551–554.

McGee, L. E., Smith, I. E. M., Millet, M.-A., Handley, H. K. & Lindsay, J. M. (2013). Asthenospheric control of melting processes in a Monogenetic Basaltic System: a case study of the Auckland Volcanic Field, New Zealand. *Journal of Petrology* **54**, 2125–2153.

Melchiorre, M., Coltorti, M., Bonadiman, C., Faccini, B., O'Reilly, S. Y. & Pearson, N. J. (2011). The role of eclogite in the rift-related metasomatism and Cenozoic magmatism of Northern Victoria Land, Antarctica. *Lithos* **124**, 319–330.

Melluso, L., Morra, V., Riziky, H., Veloson, J., Lustrino, M., Del Gatto, L. & Modeste, V. (2007). Petrogenesis of a basanite–-tephrite–phonolite volcanic suite in the Bobaomby (Cap d'Ambre) peninsula, northern Madagascar. *Journal of African Earth Sciences* **49**, 29–42.

Melluso, L., Tucker, R. D., Cucciniello, C., le Roex, A. P., Morra, V., Zanetti, A. & Rakotoson, R. L. (2018). The magmatic evolution and genesis of the Quaternary basanite-trachyphonolite suite of Itasy (Madagascar) as inferred by geochemistry, Sr-Nd-Pb isotopes and trace element distribution in coexisting phases. *Lithos* **310-311**, 50–64.

Mori, Y. (2005). X-ray fluorescence analysis of major and trace elements in silicate rocks using 1:5 dilution glass beads. *Bulletin of the Kitakyushu Museum of Natural History and Human History, Series A* **3**, 1–12.

Morimoto, N. (1988). Nomenclature of pyroxenes. *Mineralogy and Petrology* **39**, 55–76.

Moussallam, Y., Oppenheimer, C., Scaillet, B. & Kyle, P. R. (2013). Experimental Phase-equilibrium Constraints on the Phonolite Magmatic System of Erebus Volcano, Antarctica. *Journal of Petrology* **54**, 1285–1307.

Narcisi, B., Proposito, M. & Frezzotti, M. (2001). Ice record of a 13th century explosive volcanic eruption in northern Victoria Land, East Antarctica. *Antarctic Science* **13**, 174–181.

Narcisi, B., Petit, J. R., Langone, A. & Stenni, B. (2016). A new Eemian record of Antarctic tephra layers retrieved from the Talos Dome ice core (Northern Victoria Land). *Global and Planetary Change* **137**, 69–78.

Narcisi, B., Petit, J. R., Delmonte, B., Scarchilli, C. & Stenni, B. (2012). A 16, 000-yr tephra framework for the Antarctic ice sheet: a contribution from the new Talos Dome core. *Quaternary Science Reviews* **49**, 52–63.

Nardini, I., Armienti, P., Rocchi, S., Dallai, L. & Harrison, D. (2009). Sr-Nd-Pb-He-O Isotope and Geochemical Constraints on the Genesis of Cenozoic Magmas from the West Antarctic Rift. *Journal of Petrology* **50**, 1359–1375.

Nathan, S. & Schulte, F. (1968). Geology and petrology of the Campbell—Aviator Divide, Northern Victoria Land,

Antarctica: part 1—post Paleozoic rocks. *New Zealand Journal of Geology and Geophysics* **11**, 940–975.

Nekvasil, H., Dondolini, A., Horn, J., Filiberto, J., Long, H. & Lindsley, D. H. (2004). The origin and evolution of silica-saturated alkalic suites: an experimental study. *Journal of Petrology* **45**, 693–721.

Oppenheimer, C., Moretti, R., Kyle, P. R., Eschenbacher, A., Lowenstern, J. B., Hervig, R. L. & Dunbar, N. W. (2011). Mantle to surface degassing of alkalic magmas at Erebus volcano, Antarctica. *Earth and Planetary Science Letters* **306**, 261–271.

O'Reilly, S. Y. & Griffin, W. (1988). Mantle metasomatism beneath western Victoria, Australia: I. Metasomatic processes in Cr-diopside lherzolites. *Geochimica et Cosmochimica Acta* **52**, 433–447.

Paces, J. B. & Miller, J. D. (1993). Precise U-Pb ages of Duluth complex and related mafic intrusions, northeastern Minnesota: geochronological insights to physical, petrogenetic, paleomagnetic, and tectonomagmatic processes associated with the 1.1 Ga midcontinent rift system. *Journal of Geophysical Research: Solid Earth* **98**, 13997–14013.

Palmeri, R. (1997). PT paths and migmatite formation: an example from Deep Freeze Range, northern Victoria Land, Antarctica. *Lithos* **42**, 47–66.

Panter, K. S., Kyle, P. R. & Smellie, J. L. (1997). Petrogenesis of a phonolite–trachyte succession at Mount Sidley, Marie Byrd Land, Antarctica. *Journal of Petrology* **38**, 1225–1253.

Panter, K. S., Hart, S. R., Kyle, P., Blusztanjn, J. & Wilch, T. (2000). Geochemistry of Late Cenozoic basalts from the Crary Mountains: characterization of mantle sources in Marie Byrd Land, Antarctica. *Chemical Geology* **165**, 215–241.

Panter, K. S., Blusztajn, J., Hart, S. R., Kyle, P. R., Esser, R. & McIntosh, W. C. (2006). The origin of HIMU in the SW Pacific: evidence from intraplate volcanism in southern New Zealand and Subantarctic Islands. *Journal of Petrology* **47**, 1673–1704.

Panter, K. S., Castillo, P., Krans, S., Deering, C., McIntosh, W. C., Valley, J. W., Kitajima, K., Kyle, P. R., Hart, S. R. & Blusztajn, J. (2018). Melt origin across a rifted continental margin: a case for subduction-related metasomatic agents in the lithospheric source of alkaline basalt, northwest Ross Sea, Antarctica. *Journal of Petrology* **59**, 517–558.

Peccerillo, A., Donati, C., Santo, A. P., Orlando, A., Yirgu, G. & Ayalew, D. (2007). Petrogenesis of silicic peralkaline rocks in the Ethiopian rift: geochemical evidence and volcanological implications. *Journal of African Earth Sciences* **48**, 161–173.

Perinelli, C., Armienti, P. & Dallai, L. (2006). Geochemical and O-isotope constraints on the evolution of lithospheric mantle in the Ross Sea rift area (Antarctica). *Contributions to Mineralogy and Petrology* **151**, 245–266.

Perinelli, C., Armienti, P. & Dallai, L. (2011). Thermal evolution of the lithosphere in a rift environment as inferred from the geochemistry of mantle cumulates, Northern Victoria Land, Antarctica. *Journal of Petrology* **52**, 665–690.

Pfänder, J. A., Jung, S., Münker, C., Stracke, A. & Mezger, K. (2012). A possible high Nb/Ta reservoir in the continental lithospheric mantle and consequences on the global Nb budget–evidence from continental basalts from Central Germany. *Geochimica et Cosmochimica Acta* **77**, 232–251.

Pilet, S. (2015). Generation of low-silica alkaline lavas: petrological constraints, models, and thermal implications. *Geological Society of America Special Papers* **514**, SPE514–SPE517.

Pilet, S., Baker, M. B. & Stolper, E. M. (2008). Metasomatized lithosphere and the origin of alkaline lavas. *Science (New York, N.Y.)* **320**, 916–919.

Pilet, S., Baker, M. B., Müntener, O. & Stolper, E. M. (2011). Monte Carlo simulations of metasomatic enrichment in the lithosphere and implications for the source of alkaline basalts. *Journal of Petrology* **52**, 1415–1442.

Prytulak, J. & Elliott, T. (2007). TiO2 enrichment in ocean island basalts. *Earth and Planetary Science Letters* **263**, 388–403.

Putirka, K. D. (2008). Thermometers and barometers for volcanic systems. *Reviews in Mineralogy and Geochemistry* **69**, 61–120.

Putirka, K. D. (2017). Down the crater: where magmas are stored and why they erupt. *Elements* **13**, 11–16.

Putirka, K. D., Mikaelian, H., Ryerson, F. & Shaw, H. (2003). New clinopyroxene-liquid thermobarometers for mafic, evolved, and volatile-bearing lava compositions, with applications to lavas from Tibet and the Snake River Plain, Idaho. *American Mineralogist* **88**, 1542–1554.

Rasmussen, D. J., Kyle, P. R., Wallace, P. J., Sims, K. W. W., Gaetani, G. A. & Phillips, E. H. (2017). Understanding degassing and transport of CO_2-rich alkalic magmas at Ross Island, Antarctica using olivine-hosted melt inclusions. *Journal of Petrology* **58**, 841–861.

Riddolls, B. W. & Hancox, G. T. (1968). The geology of the upper Mariner Glacier region, North Victoria Land, Antarctica. *New Zealand Journal of Geology and Geophysics* **11**, 881–899.

Rocchi, S., Armienti, P. & Di Vincenzo, G. (2005). No plume, no rift magmatism in the West Antarctic Rift. *Geological Society of America Special Papers* **388**, 435–447.

Rocchi, S., LeMasurier, W. E. & Di Vincenzo, G. (2006). Oligocene to Holocene erosion and glacial history in Marie Byrd Land, West Antarctica, inferred from exhumation of the Dorrel Rock intrusive complex and from volcano morphologies. *Geological Society of America Bulletin* **118**, 991–1005.

Rocchi, S., Bracciali, L., Di Vincenzo, G., Gemelli, M. & Ghezzo, C. (2011). Arc accretion to the early Paleozoic Antarctic margin of Gondwana in Victoria Land. *Gondwana Research* **19**, 594–607.

Rocchi, S., Armienti, P., D'Orazio, M., Tonarini, S., Wijbrans, J. R. & Di Vincenzo, G. (2002). Cenozoic magmatism in the western Ross Embayment: role of mantle plume versus plate dynamics in the development of the West Antarctic Rift System. *Journal of Geophysical Research: Solid Earth* **107**, ECV 5-1–ECV 5-22.

Rocholl, A., Stein, M., Molzahn, M., Hart, S. & Wörner, G. (1995). Geochemical evolution of rift magmas by progressive tapping of a stratified mantle source beneath the Ross Sea Rift, Northern Victoria Land, Antarctica. *Earth and Planetary Science Letters* **131**, 207–224.

Rogers, N. (2006). Basaltic magmatism and the geodynamics of the East African Rift System. *Geological Society, London, Special Publications* **259**, 77–93.

Rooney, T. O., Nelson, W. R., Dosso, L., Furman, T. & Hanan, B. (2014). The role of continental lithosphere metasomes in the production of HIMU-like magmatism on the northeast African and Arabian plates. *Geology* **42**, 419–422.

Rudnick, R. L. & Gao, S. (2003). Composition of the continental crust. *Treatise on Geochemistry* **3**, 659.

Sato, K., Katsura, T. & Ito, E. (1997). Phase relations of natural phlogopite with and without enstatite up to 8 GPa: implication for mantle metasomatism. *Earth and Planetary Science Letters* **146**, 511–526.

Schneider, K. P., Kirchenbaur, M., Fonseca, R. O. C., Kasper, H. U., Münker, C. & Froitzheim, N. (2016). Role of crustal assimilation and basement compositions in the petrogenesis of differentiated intraplate volcanic rocks: a case study from the Siebengebirge Volcanic Field, Germany. *Contributions to Mineralogy and Petrology* **171**, 58.

Schroeder, D. M., Blankenship, D. D., Young, D. A. & Quartini, E. (2014). Evidence for elevated and spatially variable geothermal flux beneath the West Antarctic Ice Sheet. *Proceedings of the National Academy of Sciences* **111**, 9070–9072.

Schubert, S., Jung, S., Pfänder, J. A., Hauff, F. & Garbe-Schönberg, D. (2015). Petrogenesis of tertiary continental intra-plate lavas between Siebengebirge and Westerwald, Germany: constraints from trace element systematics and Nd, Sr and Pb isotopes. *Journal of Volcanology and Geothermal Research* **305**, 84–99.

Scott, J., Turnbull, I., Auer, A. & Palin, J. (2013). The sub-Antarctic Antipodes Volcano: a <0.5 Ma HIMU-like Surtseyan volcanic outpost on the edge of the Campbell Plateau, New Zealand. *New Zealand Journal of Geology and Geophysics* **56**, 134–153.

Scott, J. M., Hodgkinson, A., Palin, J., Waight, T. E., Van der Meer, Q. & Cooper, A. (2014). Ancient melt depletion overprinted by young carbonatitic metasomatism in the New Zealand lithospheric mantle. *Contributions to Mineralogy and Petrology* **167**, 963.

Scott, J. M., Brenna, M., Crase, J. A., Waight, T. E., van der Meer, Q. H., Cooper, A. F., Michael Palin, J., Le Roux, P. & Münker, C. (2016). Peridotitic lithosphere metasomatized by volatile-bearing melts, and its association with intraplate alkaline HIMU-like magmatism. *Journal of Petrology* **57**, 2053–2078.

Shen, W., Wiens, D. A., Stern, T., Anandakrishnan, S., Aster, R. C., Dalziel, I., Hansen, S., Heeszel, D. S., Huerta, A., Nyblade, A., Wilson, T. J. & Winberry, J. P. (2018). Seismic evidence for lithospheric foundering beneath the southern Transantarctic Mountains, Antarctica. *Geology* **46**, 71–74.

Shibata, T. & Yoshikawa, M. (2004). Precise isotope determination of trace amounts of Nd in magnesium-rich samples. *Journal of the Mass Spectrometry Society of Japan* **52**, 317–324.

Sieminski, A., Debayle, E. & Lévêque, J.-J. (2003). Seismic evidence for deep low-velocity anomalies in the transition zone beneath West Antarctica. *Earth and Planetary Science Letters* **216**, 645–661.

Sims, K. W. W., Blichert-Toft, J., Kyle, P. R., Pichat, S., Gauthier, P.-J., Blusztajn, J., Kelly, P., Ball, L. & Layne, G. (2008). A Sr, Nd, Hf, and Pb isotope perspective on the genesis and long-term evolution of alkaline magmas from Erebus volcano, Antarctica. *Journal of Volcanology and Geothermal Research* **177**, 606–618.

Sobolev, A. V., Hofmann, A. W., Sobolev, S. V. & Nikogosian, I. K. (2005). An olivine-free mantle source of Hawaiian shield basalts. *Nature* **434**, 590–597.

Sprung, P., Schuth, S., Münker, C. & Hoke, L. (2007). Intraplate volcanism in New Zealand: the role of fossil plume material and variable lithospheric properties. *Contributions to Mineralogy and Petrology* **153**, 669–687.

Stacey, J. T. & Kramers, J. (1975). Approximation of terrestrial lead isotope evolution by a two-stage model. *Earth and Planetary Science Letters* **26**, 207–221.

Storey, B. C., Leat, P. T., Weaver, S. D., Pankhurst, R. J., Bradshaw, J. D. & Kelley, S. (1999). Mantle plumes and Antarctica-New Zealand rifting: evidence from mid-Cretaceous mafic dykes. *Journal of the Geological Society* **156**, 659–671.

Storti, F., Balestrieri, M. L., Balsamo, F. & Rossetti, F. (2008). Structural and thermochronological constraints to the evolution of the West Antarctic Rift System in central Victoria Land. *Tectonics* **27**, TC4012.

Storti, F., Rossetti, F., Läufer, A. L. & Salvini, F. (2006). Consistent kinematic architecture in the damage zones of intraplate strike-slip fault systems in North Victoria Land, Antarctica and implications for fault zone evolution. *Journal of Structural Geology* **28**, 50–63.

Storti, F., Salvini, F., Rossetti, F. & Phipps Morgan, J. (2007). Intraplate termination of transform faulting within the Antarctic continent. *Earth and Planetary Science Letters* **260**, 115–126.

Sudo, A. & Tatsumi, Y. (1990). Phlogopite and K-amphibole in the upper mantle: implication for magma genesis in subduction zones. *Geophysical Research Letters* **17**, 29–32.

Sun, S. S. & Hanson, G. N. (1975). Origin of Ross Island basanitoids and limitations upon the heterogeneity of mantle sources for alkali basalts and nephelinites. *Contributions to Mineralogy and Petrology* **52**, 77–106.

Talarico, F., Borsi, L. & Lombardo, B. (1995). Relict granulites in the Ross Orogen of northern Victoria Land (Antarctica), II. Geochemistry and palaeo-tectonic implications. *Precambrian Research* **75**, 157–174.

ten Brink, U. S., Hackney, R. I., Bannister, S., Stern, T. A. & Makovsky, Y. (1997). Uplift of the Transantarctic Mountains and the bedrock beneath the East Antarctic ice sheet. *Journal of Geophysical Research: Solid Earth* **102**, 27603–27621.

Thompson, G., Smith, I. & Malpas, J. (2001). Origin of oceanic phonolites by crystal fractionation and the problem of the Daly gap: an example from Rarotonga. *Contributions to Mineralogy and Petrology* **142**, 336–346.

Tiepolo, M., Oberti, R., Zanetti, A., Vannucci, R. & Foley, S. F. (2007). Trace-element partitioning between amphibole and silicate melt. *Reviews in Mineralogy and Geochemistry* **67**, 417–452.

Timm, C., Hoernle, K., Werner, R., Hauff, F., van den Bogaard, P., White, J., Mortimer, N. & Garbe-Schönberg, D. (2010). Temporal and geochemical evolution of the Cenozoic intraplate volcanism of Zealandia. *Earth-Science Reviews* **98**, 38–64.

van der Meer, Q., Waight, T. E., Scott, J. & Münker, C. (2017). Variable sources for Cretaceous to recent HIMU and HIMU-like intraplate magmatism in New Zealand. *Earth and Planetary Science Letters* **469**, 27–41.

Varne, R. (1968). The petrology of Moroto Mountain, eastern Uganda, and the origin of nephelinites. *Journal of Petrology* **9**, 169–190.

Vignaroli, G., Balsamo, F., Giordano, G., Rossetti, F. & Storti, F. (2015). Miocene-to-Quaternary oblique rifting signature in the Western Ross Sea from fault patterns in the McMurdo Volcanic Group, north Victoria Land, Antarctica. *Tectonophysics* **656**, 74–90.

Villemant, B., Jaffrezic, H., Joron, J.-L. & Treuil, M. (1981). Distribution coefficients of major and trace elements; fractional crystallization in the alkali basalt series of Chaîne des Puys (Massif Central, France). *Geochimica et Cosmochimica Acta* **45**, 1997–2016.

Watson, T., Nyblade, A., Wiens, D. A., Anandakrishnan, S., Benoit, M., Shore, P. J., Voigt, D. & VanDecar, J. (2006). P and S velocity structure of the upper mantle beneath the Transantarctic Mountains, East Antarctic craton, and Ross Sea from travel time tomography. *Geochemistry, Geophysics, Geosystems* **7**, Q07005.

Weaver, S., Bradshaw, J. & Laird, M. (1984). Geochemistry of Cambrian volcanics of the Bowers Supergroup and implications for the Early Palaeozoic tectonic evolution of northern Victoria Land, Antarctica. *Earth and Planetary Science Letters* **68**, 128–140.

Weaver, S., Storey, B., Pankhurst, R., Mukasa, S., DiVenere, V. & Bradshaw, J. (1994). Antarctica-New Zealand rifting and Marie Byrd Land lithospheric magmatism linked to ridge subduction and mantle plume activity. *Geology* **22**, 811–814.

Weaver, S. D., Saunders, A. D., Pankhurst, R. J. & Tarney, J. (1979). A geochemical study of magmatism associated with the initial stages of back-arc spreading. *Contributions to Mineralogy and Petrology* **68**, 151–169.

Whitaker, M. L., Nekvasil, H., Lindsley, D. H. & Difrancesco, N. J. (2006). The role of pressure in producing compositional diversity in intraplate basaltic magmas. *Journal of Petrology* **48**, 365–393.

White, J. C., Espejel-García, V. V., Anthony, E. Y. & Omenda, P. (2012). Open system evolution of peralkaline trachyte and phonolite from the Suswa volcano, Kenya rift. *Lithos* **152**, 84–104.

Wilson, G. S., Lavelle, M., McIntosh, W. C., Roberts, A. P., Harwood, D. M., Watkins, D. K., Villa, G., Bohaty, S. M., Fielding, C. R., Florindo, F., Sagnotti, L., Naish, T. R., Scherer, R. P. & Verosub, K. L. (2002). Integrated chronostratigraphic calibration of the Oligocene-Miocene boundary at 24.0 ± 0.1 Ma from the CRP-2A drill core, Ross Sea, Antarctica. *Geology* **30**, 1043–1046.

Wilson, M., Downes, H. & Cebria, J.-M. (1995). Contrasting fractionation trends in coexisting continental alkaline magma series; Cantal, Massif Central, France. *Journal of Petrology* **36**, 1729–1753.

Winberry, J. P. & Anandakrishnan, S. (2004). Crustal structure of the West Antarctic rift system and Marie Byrd Land hotspot. *Geology* **32**, 977–980.

Zindler, A. & Hart, S. (1986). Chemical geodynamics. *Annual Review of Earth and Planetary Sciences* **14**, 493–571.

Zipfel, J. & Wörner, G. (1992). Four-and five-phase peridotites from a continental rift system: evidence for upper mantle uplift and cooling at the Ross Sea margin (Antarctica). *Contributions to Mineralogy and Petrology* **111**, 24–36.